Investigating the metabolic load of monoclonal antibody production conveyed to an inducible CHO cell line using a transfer-rate online monitoring system

Sebastian-Juan Reyes [a,b], Lucas Lemire [a,b], Yves Durocher [a], Robert Voyer [a], Olivier Henry [b,*], Phuong Lan Pham [a,*]

[a] *Human Health Therapeutics Research Centre, National Research Council Canada, 6100 Royalmount Avenue, Montréal, Quebec H4P 2R2, Canada*
[b] *Department of Chemical Engineering, Polytechnique Montreal, Montreal, Quebec H3T 1J4, Canada*

ARTICLE INFO

ABSTRACT

Shake flasks are a foundational tool in early process development by allowing high throughput exploration of the design space. However, lack of online data at this scale can hamper rapid decision making. Oxygen transfer rate (OTR) monitoring has been readily applied as an online process characterization tool at the benchtop bioreactor scale. Recent advances in modern sensing technology have allowed OTR monitoring to be available at the shake flask level. It is now possible to multiplex time-of-action (e.g., Induction, temperature shift, pH shift, feeding initiation, point of harvest) characterization studies by relying on careful analysis of OTR profile kinetics. As a result, there is potential to save time and capital expenditures while exploring process intensification studies though accurate and physiologically relevant online data. In this article, we detail the application of OTR monitoring to characterize the impact that recombinant protein production has on an inducible CHO cell line expressing Palivizumab. We then test out time-of-action studies to intensify protein production outcomes. We observe that recombinant protein expression causes a metabolic load that diminishes potential biomass growth. As a result, when compared to a control standard process, delaying induction and temperature shift has the potential to improve viable cell densities (VCD) by 2-fold thus increasing recombinant protein yield by over 30 %. The study also demonstrates that OTR can serve as a useful tool to detect cessation of exponential growth. Consequently, time-of-action points that are characteristic of inducible systems can be formulated accurately and reliably to maximize production performance.

1. Introduction

Shake flaks have been widely used in the biotechnology industry since the 1930's when Kluyver and Perquin began fermentation of fungus in shake flasks (Anderlei et al., 2004). They are an efficient tool for screening large amounts of strains or cell lines, optimizing culture conditions and media composition during the initial stages of process development (Anderlei and Büchs, 2001; Anderlei et al., 2004). As such, they permit the minimization of cost and the maximization of process information. It is estimated that 90 % of all cell culture experiments make use of shaken systems at some point in the development cycle (Anderlei et al., 2004). These shaken systems are used in tandem with shaking tables or incubator shakers since these platforms are responsible for the shaking movement that allows for the mixing and oxygen mass transfer. Shaking can be done through rotatory shaking, linear reciprocating, and orbital shaking (Doran, 1995). The incubators have the added benefit of maintaining commonly a 5 % CO_2 atmosphere that is critical for culturing mammalian cell lines (Hoshan et al., 2019). However, lack of on-line data is an issue on these shaken flasks and as such, it can sometimes behave as a black box where little is known about the mass transfer and mixing within the system. Recent industry-wide pushes towards Biopharma 4.0 have meant that increased monitoring and control capabilities are possible in stirred tank bioreactors with strategies based on hardware and software-based sensors (Reyes et al., 2022; Reyes et al., 2024). A relevant monitoring parameter that has gained prominence among these strategies in process development is oxygen uptake rate (OUR) given its ease of estimation through various methods (Fontova et al., 2018; Goh et al., 2020; Martínez-Monge et al.,

---

2019; Wallocha and Popp, 2021). Most noteworthy is its ability to provide information regarding the metabolic state of the culture (Europa et al., 2000; Lin et al., 2002; Zhou and Hu, 1994; Zhou et al., 1995). Thanks to these characteristics, OUR has been used in tandem with correlations to develop dynamic feeding strategies (Casablancas et al., 2013; Goldrick et al., 2018; Martínez-Monge et al., 2018; Reyes, Pham, et al., 2024) as well as detect nutrient limitations (Zalai et al., 2016) and evaluate the impact of media additives (Huang et al., 2010). Additionally, OUR has also shown great correlation with both viable cell density and viable cell volume (Pappenreiter et al., 2019) along with an ability to estimate the cessation of exponential growth phase (Ducommun et al., 2000; Reyes et al., 2023). Given these features, OUR has been used as a basis for time-of-action events where time of harvest or time of infection (in viral production) can be determined based on changes in the slope of the OUR curve in batch, fed-batch, and perfusion configurations (Gálvez et al., 2012; Kussow et al., 1995; Lecina et al., 2006).

Initially, to properly study the environment within the shake flasks and in consequence accurately study the microbial cultures inside them, an oxygen transfer rate (OTR) device was developed by Anderlei and Buchs denominated the RAMOS (respirator monitoring system) (Anderlei and Büchs, 2001; Anderlei et al., 2004; Hansen et al., 2012). In their work, the estimation of the OTR was realized online, allowing measurements to be done under sterile conditions as well as under a suitable mixing environment (shaken). The carbon dioxide transfer rate (CTR) along with the respiratory quotient (RQ = CO_2 produced / O_2 consumed) could also be estimated using their proposed technique. Since the shake flask system is considered to be in a pseudo steady state, the dynamics of mass transfer are more rapid than the changes in oxygen requirement of the cell culture. In consequence, oxygen transfer rate (OTR) is roughly approximated to oxygen uptake rate (OUR), while the carbon dioxide transfer rate (CTR) also comes close to carbon dioxide evolution rate (CER) (He et al., 2019). This would indicate that OUR = OTR and that CER = CTR (He et al., 2019). However, careful consideration and validation must be realized with the assumption that CER = CTR since carbon dioxide sources within the mammalian cell culture system include cellular respiration and the sodium bicarbonate/carbonate buffer medium (Goudar et al., 2011).

These characteristics have led to widespread use of the RAMOS system in a variety of biotechnological applications (Anderlei and Büchs, 2001; Anderlei et al., 2004; Guez et al., 2008; Hansen et al., 2012; Losen et al., 2004; Rechmann et al., 2007; Seletzky et al., 2007; Seletzky et al., 2007; Stöckmann et al., 2003; Zimmermann et al., 2006). The RAMOS system has also been used concomitantly with an on-line fiber-optic pH measuring system to produce more information about the fermentation cycle (Scheidle et al., 2007). It was determined that accurate online monitoring for pH and dissolved oxygen (DO) in shake flask cultures was possible since all values fell within 4 % of the experimentally determined offline values. The same principle of the RAMOS system has also been applied to 48- and 96-well microtiter plates (Dinger et al., 2022; Ihling et al., 2023). Adaptation to the RAMOS systems has been made to reproducibly monitor the oxygen consumption of mammalian cells in shake flasks, demonstrating correlations with cell viability, cellular density, and depletion of carbon sources (Ihling et al., 2021; Ihling, Munkler, Paul, Berg, et al., 2022; Ihling et al., 2022).

Within a shake flask system, it has been established that numerous parameters effect the oxygen mass transfer such as the flask shape, flask size, vented cap, shaking frequency, shaking diameter, filling volume, and surface material properties of the shake flask (Maier and Büchs, 2001; Maier et al., 2004). The hydrodynamics of said OTR revolve around the formation of a liquid film that is distributed along the flask wall as the sickle rotates within the flask (Maier and Büchs, 2001; Maier et al., 2004). Thus, the relevant mass transfer area within the shaken system is made up of two equally important components, the mass transfer area of the liquid surface and the area of the liquid film that is formed on the flask wall (Maier and Büchs, 2001; Maier et al., 2004). It must be noted that within these systems, 'in-phase' and 'out-of-phase'

phenomena may occur (Klöckner et al., 2013). Out-of-phase behaviour occurs when the liquid no longer rotates along the direction of the centrifugal acceleration (Klöckner et al., 2013). In contrast, 'in-phase' phenomenon is characterized by a rotating liquid that forms thin films along the flask surface in a continuous manner which is optimal for mass transfer within the shaken system (Klöckner et al., 2013). Alternatively, it has also been determined that an increased shaking rate can result in higher shear stress which can be detrimental to shear-sensitive cell cultures (Mancilla et al., 2015). As such, making sure that OTR_{max} is always superior to OUR_{max} is important to not have an oxygen limited system while still in keeping with shear related constraints. This is especially relevant when increased cell densities are reached thanks to process intensification strategies, since very high cellular concentrations mean increased volumetric oxygen consumption. Consequently, improved understanding of these foundational shaken systems is critical to develop strategies that can be extrapolated outside the milli-litre scale into large-scale production platforms. In this paper, the characterization of a fed-batch process through OTR estimation in a shaken system is detailed and utilized as a basis for process intensification through time-of-action studies to augment Palivizumab yield; the latter is a monoclonal antibody commonly used to prevent serious lung diseases in infants caused by respiratory syncytial virus (RSV) (Moore et al., 2022).

2. Materials and methods

2.1. Induction vs no induction

A proprietary CHO-GS stable cell line expressing Palivizumab was grown in BalanCD CHO Growth A medium (Fujifilm/Irvine Scientific) supplemented with 50 μM MSX (L-Methionine sulfoximine, Sigma-Aldrich) and 0.1 % (w/v) Kolliphor P188 (Sigma-Aldrich) for cell maintenance and seed train expansion. Inducible stable cell lines in CHO cells have been demonstrated to effectively express the SARS-CoV-2 spike protein and rituximab using the cumate gene switch system, which originates from the cymene operon of *Pseudomonas putida* (Joubert et al., 2023; Mellahi et al., 2019). In essence, rCymR is linked with an activation domain (VP16) to create the reverse cumate activator (rcTA), which triggers transcription in the presence of cumate but not in its absence (Mullick et al., 2006). This means cumate alters the shape of the chimeric molecule. Without cumate, rcTA cannot bind to the operator sites; however, when cumate is available, rcTA can bind correctly to the operator sites and initiate activation.

For the induction vs. non induction experiment (Table 1), the 250-mL Corning flasks (6 total in triplicate) were shaken in parallel at 200 rpm (25 mm orbital diameter) in a Kuhner ISF1-X at 37°C, 5 % CO_2, and 75 % relative humidity. Half of the flasks (3) were induced, and the other half remained un-induced throughout the experiment. The flasks were connected to the Transfer-rate Online Monitoring (TOM) system (Kuhner Inc., Switzerland) via the Corning flask's adapters for Oxygen Transfer Rate (OTR) measurements. Each flask was seeded at 0.4×10^6 cells/mL with a filling volume of 50 mL and cultivated for 17 days. Temperature downshift (37°C to 32°C) was realized 5 days after seeding (or 2 days post-induction (dpi) for inducible cases). Induction was performed with the addition of 4-Isopropylbenzenecarboxylate (Cumate, ArkPham) 3 days after seeding at a concentration of 2 μg/mL. All six cultures were fed with BalanCD CHO Feed 4 (Fujifilm/Irvine Scientific) and supplemented with glucose to maintain the concentration above 17 mM (3.06 g/L). Glucose supplementation relied on estimating

Table 1
Induction vs no-induction experimental condition (6 flasks in triplicate).

Flask ID	Seeding Density ($\times 10^6$ cells/mL)	Cumate Addition	Induction Day (Dpi)	Temperature Shift Day (Dpi or Day)
1–3	0.4	Yes	0 dpi	2 dpi
4–6	0.4	No	N/A	Day 5

glucose consumption between sampling days and extrapolating the observed glucose consumption for the next sampling period. Consequently, enough glucose is added to counteract the expected glucose consumption such that the residual glucose is maintained above 17 mM. Feed 4 supplementation was realized on 0, 2, 4, 7, 9,11 dpi at 5 %, 7.5 %, 7.5 %, 5 %, 5 %, 7.5 % of initial culture volume (37.5 % total). 1-mL samples were taken from the flasks on days −3, 0, 2, 4, 7, 9, 11, and 14 dpi for off-line analysis, while feeding was realized from 0 dpi (day 3) onward. Cell density, viability, and main metabolites (glucose, lactate, ammonia) were measured utilizing the previously reported methodology (Joubert et al., 2023; Poulain et al., 2017; Stuible et al., 2021). OTR of cell cultures in shake flasks was measured using the TOM system. The measuring cycles of the TOM system consist of three phases. First, a base line aeration phase allows the system to re-create standard shake flask aeration conditions which is using air from the incubator atmosphere that contains 5 % CO_2. A measurement phase is followed in which aeration is stopped in order to measure oxygen consumption and carbon dioxide generation inside the closed system. Finally, a recovery phase aerates the cell culture to protect the physiological integrity of the cell cultures as well as aid in the calibration of the O_2 electrochemical sensors. Each measuring phase generates a single data point from which the OTR curve can be produced. An aeration flow rate of air at 16 mL/min was maintained throughout the run during the aeration phase that best re-creates standard shake flask aeration condition. OTR measurements were carried out over 105 min, comprising of 64 min of standard shake flask aeration re-creation, 35 min of measurement time, and 6 min of high-flow flushing time to bring the oxygen concentrations back to steady state. Various conditions will be evaluated, including the effects of induction versus no induction, temperature shifts during induction, to determine their impact on overall process performance. Amino acid measurements were conducted following the AccQ-Tag Ultra Derivatization Kit protocol (Waters Corporation, USA) that employs an AccQ-Tag Ultra C18 column with the ACQUITY H-Class UPLC system (Waters Corporation, USA) and UV detection. mAb titers were measured using Protein A HPLC method. The supernatants were filtered through MultiScreen HV 96-well filtration plates (Durapore®, 0.45 μm, Millipore, USA) at 1500xg for 2 min to remove cellular debris. HPLC analysis was performed on a 2695/2996 HPLC system (Waters Corporation, USA) with a Protein A cartridge.

The maximum Oxygen Transfer Rate (OTR) of the shake flask system was measured using the sulfite method (Giese et al., 2014). A 0.35 M sodium sulfite solution ($\geq$ 99 %; Sigma-Aldrich) in 0.012 M phosphate buffer prepared with deionized water adjusted to pH 8 was used ($Na_2HPO_4 \geq$ 99 % purity; $NaH_2PO_4 \geq$ 99 % purity; Sigma-Aldrich). The reaction was catalyzed by 10^{-7} M cobalt sulfate ($\geq$ 99 % purity; Sigma-Aldrich). The maximum OTR measurements with the sulfite system were conducted with 250-mL shake flasks filled with 50 mL of MiliQ water shaken at 200 RPM with an orbital diameter of 25 mm.

2.2. Time of action

For the impact of time-of-action experiments (Table 2), the 8 flasks (4 conditions in duplicate) were shaken in parallel at 200 rpm (25 mm orbital diameter) in a Kuhner ISF1-X at 37°C, 5 % CO_2, and 75 % relative humidity. Each flask was seeded at 0.4×10^6 cells/mL with a filling volume of 50 mL in a 250-mL Corning shake flask. Eight flasks were induced and temperature was shifted by a pair (2 flasks) on day 5, day 6,

Table 2
Time-of-action experimental condition (8 flasks in duplicate).

Temperature Shift (Day)	Induction Time(Day)	Seeding Density(x10⁶ cells/mL)
5	5	0.4
6	6	0.4
7	7	0.4
9	9	0.4

day 7, and day 9.

The flasks were connected to the TOM system via the Corning flask's adapters. OTR of cell cultures in shake flasks was measured using the TOM system similar to what is described above. 1-mL samples were taken from the flasks on days 0, 3, 5, 7, 10, 12, 14 and 17 for off-line analysis. Cell density, viability, and main metabolites (glucose, lactate, ammonia) were measured as noted previously. Cultures were fed with BalanCD CHO Feed 4 and supplemented with glucose to maintain the concentration above 17 mM (3.06 g/L) on days 3, 5, 7, 10, 12, 14. Additional glucose monitoring and supplementation were realized when the time between feedings is longer than two days to avoid glucose depletion. Glucose supplementation relied on estimating glucose consumption between sampling days and extrapolating the observed glucose consumption for the next sampling period. Consequently, enough glucose is added to counteract the expected glucose consumption such that the residual glucose is maintained above 17 mM. Feed 4 and glucose supplementation was realized on days 3 (5 %), 5 (7.5 %), 7 (3.75 %), 9 (3.75 %), 10 (5 %), 12 (5 %), 14 (7.5 %), 16 (only glucose monitoring) for day 9 induction, days 3 (5 %), 5 (7.5 %), 7 (7.5 %), 8 (only glucose monitoring), 10 (5 %), 12 (5 %), 14 (7.5 %), 16 (only glucose monitoring) for day 7 induction, days 3 (5 %), 5 (3.75 %), 6 (3.75 %), 7 (7.5 %), 8 (only glucose monitoring), 10 (5 %), 12 (5 %), 14 (7.5 %), 16 (only glucose monitoring) for day 6 induction, days 3 (5 %), 5 (7.5 %), 7 (7.5 %), 9 (only glucose monitoring), 10 (5 %), 12 (5 %), 14 (7.5 %), 16 (only glucose monitoring) for day 5 induction. Total feed amounts (37.5 % of initial working volume) were kept constant across conditions. The 7.5 % feed of day 5 for day 6 induction and of day 7 for day 9 induction was split in half so that induction day was always accompanied by Feed 4 supplementation.

2.3. Estimated variables

The integral viable cell concentration (IVCC) and growth rate (μ) were calculated with Eqs. 1 and 2 respectively where, VCD is the viable cell density, V is the flask volume and t is the sampling time and subscript i and $i-1$ refers to the current and the previous sampling times respectively, subscript *initial* represents the first measured value:

$$IVCC = \sum \Delta IVCC = \sum_{i=1}^{n} \frac{(VCD_i \times V_i) + (VCD_{i-1} \times V_{i-1})}{2} * \frac{(t_i - t_{i-1})}{V_i} \quad (1)$$

$$\mu = \frac{in\ (VCD_i VCD)/(t_i - t_{initial})}{24} \quad (2)$$

Cell specific consumption rates of glucose (qGlu) and production of lactate (qLac), ammonia (qNH₃) and amino acids (qA_A) were calculated using Eqs. 3–6 respectively where, [Glu], [Lac], [NH₃] and [A_A] refer to the concentrations of glucose, lactate ammonia and amino acids, ΔIVCC refers to the change in integral viable cell density, and subscripts 1 and 2 refer to the previous and current sampling times respectively. For glucose and amino acids subscript 1 represents substrate concentration after feeding and subscript 2 represents spent media value of next sampling day:

$$qGlu = \frac{[Glu]_1 - [Glu]_2}{\Delta IVCC} \quad (3)$$

$$qLac = \frac{[Lac]_2 - [Lac]_1}{\Delta IVCC} \quad (4)$$

$$qNH_3 = \frac{[NH_3]_2 - [NH_3]_1}{\Delta IVCC} \quad (5)$$

$$qA\_A = \frac{[A\_A]_1 - [A\_A]_2}{\Delta IVCC} \quad (6)$$

Cell specific (qP) mAb production was calculated from Eq. 7 where P is mAb concentration, subscripts 1 and 2 refer to the previous and

current sampling times respectively. Specific respiration rates (q_{o_2}) were estimated using Eq. 8 by dividing OTR at sampling point by viable cell densities at sampling point.

$$qP = \frac{P_2 - P_1}{\Delta IVCC} \qquad (7)$$

$$q_{o_2} = \frac{OTR_i}{VCD_i} \qquad (8)$$

3. Results and discussions

3.1. Characterization of metabolic loads of induced and non-induced cell cultures

To determine the impact that recombinant protein production has on cell culture behaviour, an induction vs no-induction experiment was devised. Here, the cultures would be subjected to the same feeding strategy and temperature downshift. Thus, observed differences are interpreted as caused by recombinant protein production rather than process condition-related impacts. As can be seen in Fig. 1A, cells in the non-induced condition continue growing well after the temperature downshift at 2 dpi (day 5) indicating that cells in induced conditions have comparatively lower growth rates. This can be further discerned from Fig. 1B that cell specific growth rate remains lower in the induced

condition after 0 dpi (day 3) up until 11 dpi (day 14) despite the cultures being subjected to equal process conditions (e.g., feeding, shaking, temperature shift). Similar phenomenon has been observed in microbial cultures where growth retardation was observed to be caused by recombinant protein expression (Kafri et al., 2016; Li and Rinas, 2020). It was determined that the so-called metabolic burden was caused by recombinant protein synthesis. More precisely, the impact was attributed to rates of transcription and translation as well as processes following translation (e.g. protein folding) (Kafri et al., 2016; Li and Rinas, 2020). Similar observations have been made in mammalian cell lines, where over-expression of recombinant protein led to increased metabolic load such that maximal cell density and doubling times were impacted (Yallop and Svendsen, 2001). It is noteworthy that in cells expressing the recombinant protein, the flux of glucose was directed away from lactate production towards TCA cycle activity (Sheikholeslami et al., 2013b; Yallop and Svendsen, 2001).

As observed in Fig. 1C, non-induced cultures decrease in viability faster than the induced cultures. This may be because non-induced cultures reach about 2 times more biomass and consequently it was more difficult to sustain with the current feed supplementation protocol. As such, glucose concentrations reached above 60 mmol/L after supplementation in the non-induced cultures while induced cultures were never subjected to glucose concentrations above 35 mmol/L (data not shown). These large oscillations in nutrient concentration may have had
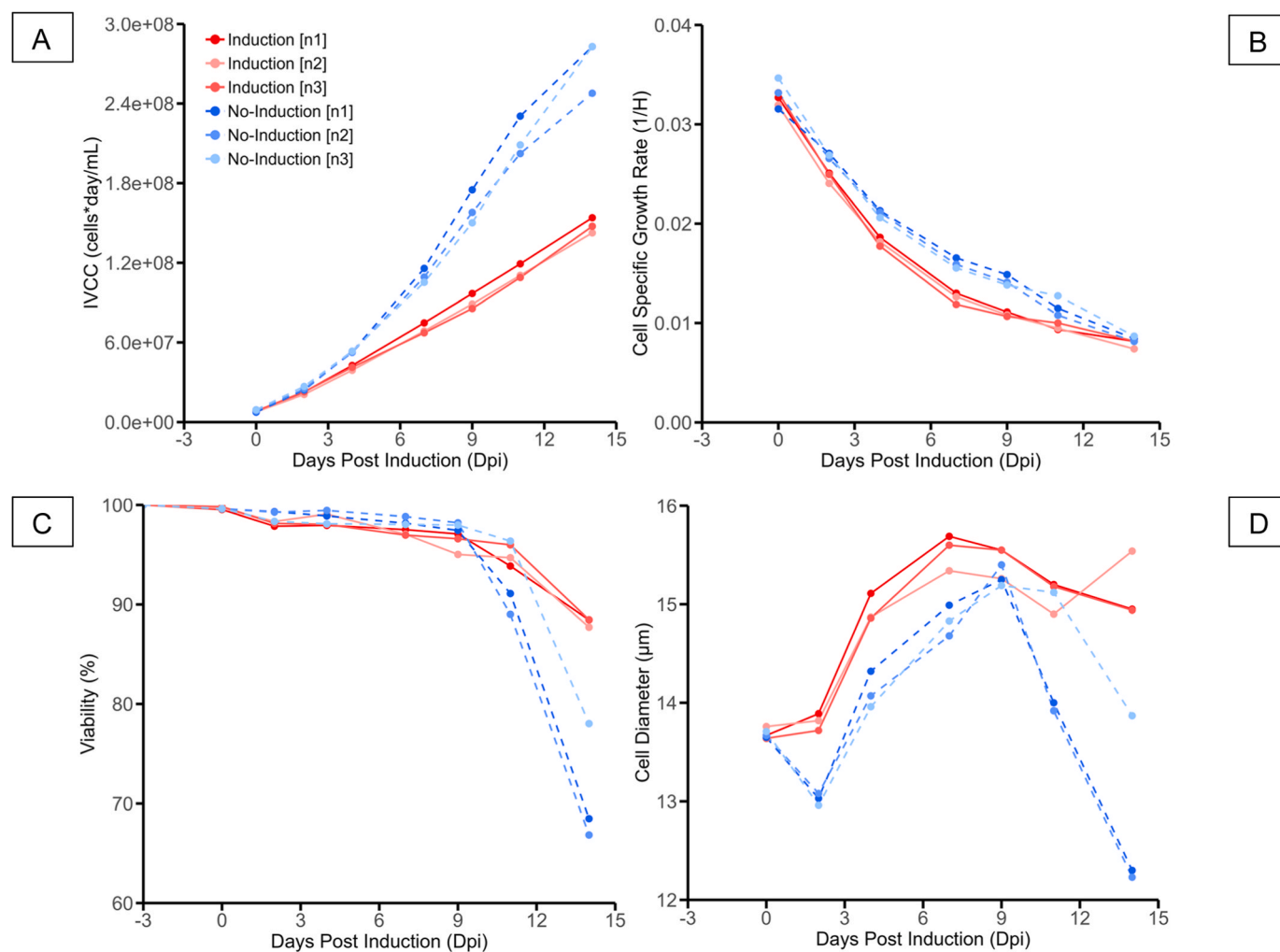
Fig. 1. Impact of induction on A) Integral Viable Cell Concentration (IVCC), B) Cell Specific Growth Rate, C) Viability, C) Cellular diameter. Two conditions were studied (induction vs no induction) in triplicate. Three cultures were subjected to cumate induction at 0 dpi (day 3) while 3 others were left without induction. A temperature downshift from 37°C to 32°C was performed at 2 dpi (day 5) for both studied conditions.

an impact on the onset of culture decline. Fig. 1D shows that cell diameter increases after the 2-dpi temperature downshift. This phenomenon has been observed in other CHO cell cultures (Huang et al., 2010; Wang et al., 2024). In the literature, it has been postulated that cell size increase and specific protein production rates are inter-related (Kim et al., 2001; Lloyd et al., 2000; Pan et al., 2017; Wagner et al., 2011). Indeed, when overlaying specific productivity with cellular diameter increase (Fig. 1S), a linear relationship can be found between 2 dpi and 11 dpi ($R^2 = 0.76$) such that increases in cell volume relate to increases in specific productivity and decreases in cell volume also show a decrease in specific productivity. Moreover, in our case, cellular diameter increase was observed for both induced and non-induced conditions indicating that cell size increase is more strongly related to temperature downshift rather than recombinant protein production itself. However, it is worth mentioning that on average, cell diameters are higher in the induced condition compared to the non induced culture. It has been suggested in the literature that the increase in cell volume is related to increases in transcription, translation, and secretion machinery that is regulated by the mechanistic target of rapamycin (mTOR) signaling pathway (Dreesen and Fussenegger, 2011; Edros et al., 2014; McVey et al., 2016). A downshift in temperature has also been shown to affect cell size in CHO cells (Martínez et al., 2015; Tait et al., 2013), with this phenomenon generally attributed to cell cycle arrest (Pan et al., 2017). Transcriptome analysis of fed-batch CHO cultures reveals that

cell cycle arrest, characterized by upregulation of cyclin-dependent kinase inhibitors and downregulation of cyclin-dependent kinases and cyclins, coincides with increased cell size (Pan et al., 2019). During this phase, synchronized activation of upstream pathways regulating mTOR promotes its activity, while downstream targets of mTOR stimulate protein translation and lipid synthesis (Pan et al., 2019). These changes can potentially augment the biosynthetic machinery (Koscielny et al., 2021) which may explain why increased cell volume has been associated with higher antibody production, as the expanded machinery could support greater synthesis and secretion efficiency. Notably, a decrease in cellular diameter is detected at the onset of decrease in viability (after 9 dpi). This phenomenon may be explained by apoptotic volume decrease. As it has been discerned that during the early stages of apoptosis, cell shrinkage and pyknosis occur (Elmore, 2007; Nunez et al., 2010). Importantly, cumate has been found to be non-toxic in CHO cell fed-batch cultures in concentrations ranging from 0.1 to 10 µg/mL (Poulain et al., 2017). The nontoxic impact of the inducer on mammalian cell growth have been further confirmed in the literature (Gaillet et al., 2010; Mullick et al., 2006). Given that induction was realized at 2 µg/mL we expect no impact from the small molecule inducer. The cumate system is important because it minimizes r-protein expression during stable CHO pool selection, reducing cellular stresses like ER stress and metabolic burden (Maltais et al., 2023). This leads to pools with a higher frequency of high-expressing cells and improved volumetric
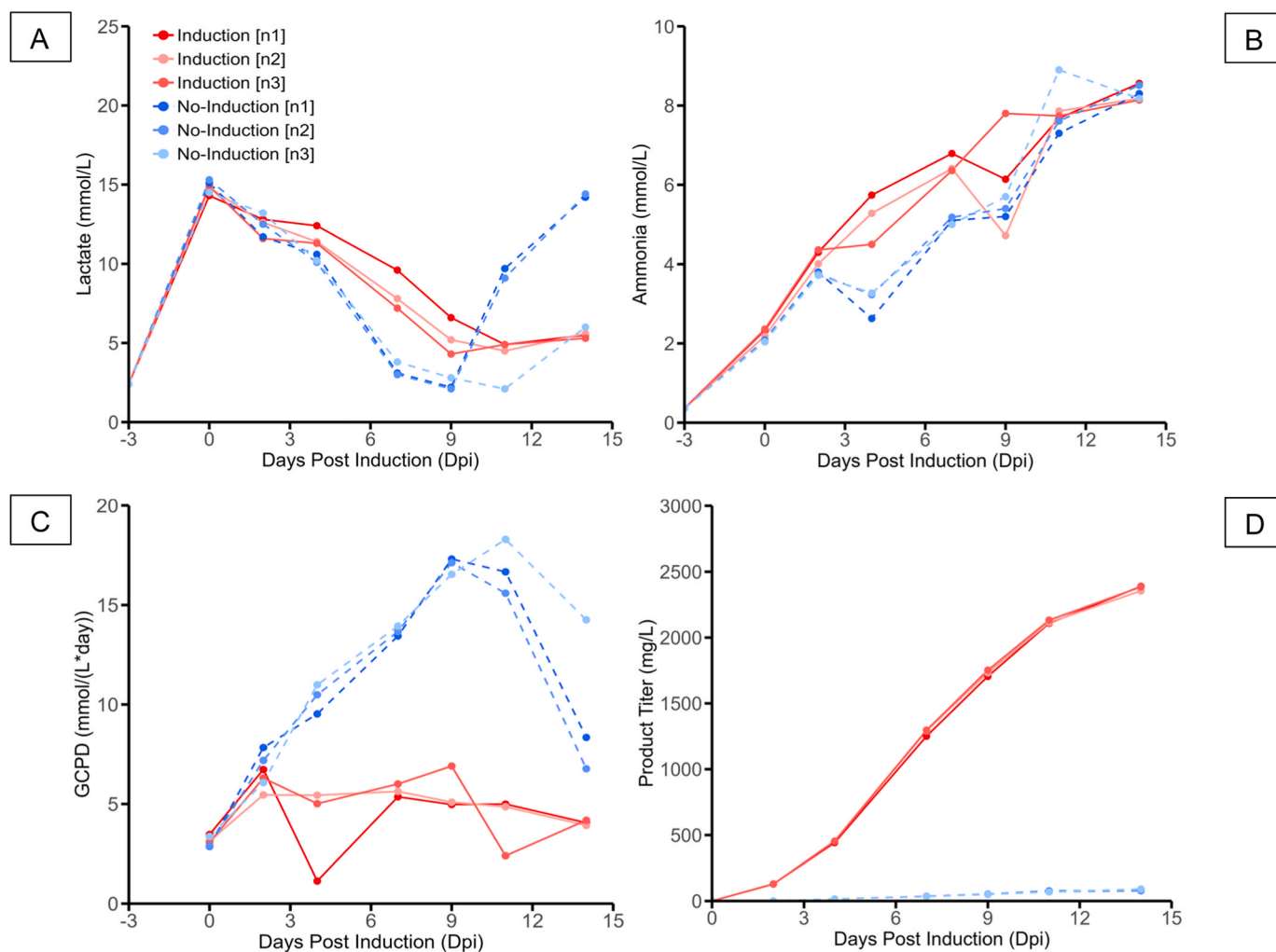

Fig. 2. Impact of production induction on A) Lactate profile, B) Ammonia profile, C) Glucose consumed per day (GCPD), D) Protein yield. Two conditions were studied (induction vs no induction) in triplicate. Three cultures were subjected to cumate induction at 0 dpi (day 3) while 3 others were left without induction. A temperature downshift from 37°C to 32°C was performed at 2 dpi (day 5) for both studied conditions.

productivity. In contrast, overexpression of the r-protein during pool selection hinders recovery and increases cell death (Poulain et al., 2019). Therefore, the cumate gene switch has been suggested in the literature as an effective platform for stable clone generation (Poulain et al., 2019).

When detailing main metabolic activity, it is possible to discover several trends. In Fig. 2A, it can be observed how the lactate concentration increases (to 15 mmol/L) until 0 dpi and begins to be consumed for both induced and non-induced conditions. The non-induced cultures (No-Induction) consume lactate until cell decline (9 dpi) at which point lactate re-production begins. When looking at the specific rates (Figure 2SA), specific lactate production remains similar in both induced and non-induced cultures until 7 dpi, at which point, non-induced specific lactate production increases with respect to the induced condition. In the literature, two states have been discerned with respect to lactate metabolism. A first state is characterized by lactate production during the first few days of the culture. This lactate accumulation is a direct consequence of high glycolytic pathway activity that is concomitant to rapid biomass growth (Hartley et al., 2018; Mulukutla et al., 2012; Ozturk et al., 1992; Pereira et al., 2018). A secondary state of lactate consumption follows the rapid cell growth. Lactate re-consumption has been commonly assumed to be a good key process indicator (KPI) given its correlation with high recombinant protein productivity (Pereira et al., 2018; Zagari et al., 2013).

When observing ammonia accumulation (Fig. 2B), the non-induced condition accumulates less ammonia when compared to the induced condition between 2 dpi and 9 dpi despite both conditions being subjected to an equal feed regimen and despite the fact that the non-induced condition has roughly 3 times more biomass (Fig. 3A). Ammonia specific rates (Figure 2SB) show, on average, lower specific ammonia production between 2 dpi to 7 dpi in non-induced cultures compared to induced cultures. Given the fact that ammonia accumulation is driven by transamination and deamination reactions of amino acids (Pereira et al., 2018), it can be hypothesised that the non-induced cultures had less amino acid catabolism, and consequently, less TCA cycle activity, since it has been noted that during protein production, TCA cycle activity is upregulated (Coulet et al., 2022; Pereira et al., 2018). It has been determined that peak growth rates are associated with high glycolytic activity and low TCA cycle activity while peak protein production is associated with low glycolytic activity and a high oxidative state (high TCA cycle activity) (Coulet et al., 2022; Templeton et al., 2013). When observing Fig. 2C, it is clear that non-induced cultures had significantly higher daily volumetric glucose consumption when compared to the induced conditions. This, in part, can be explained by the higher biomass accumulation. However, when analysing specific rates (Fig. 2SC), it can be said that on average, higher specific glucose daily consumption rates were detected in the non-induced condition when compared to its induced counterpart. This holds true even after temperature downshift
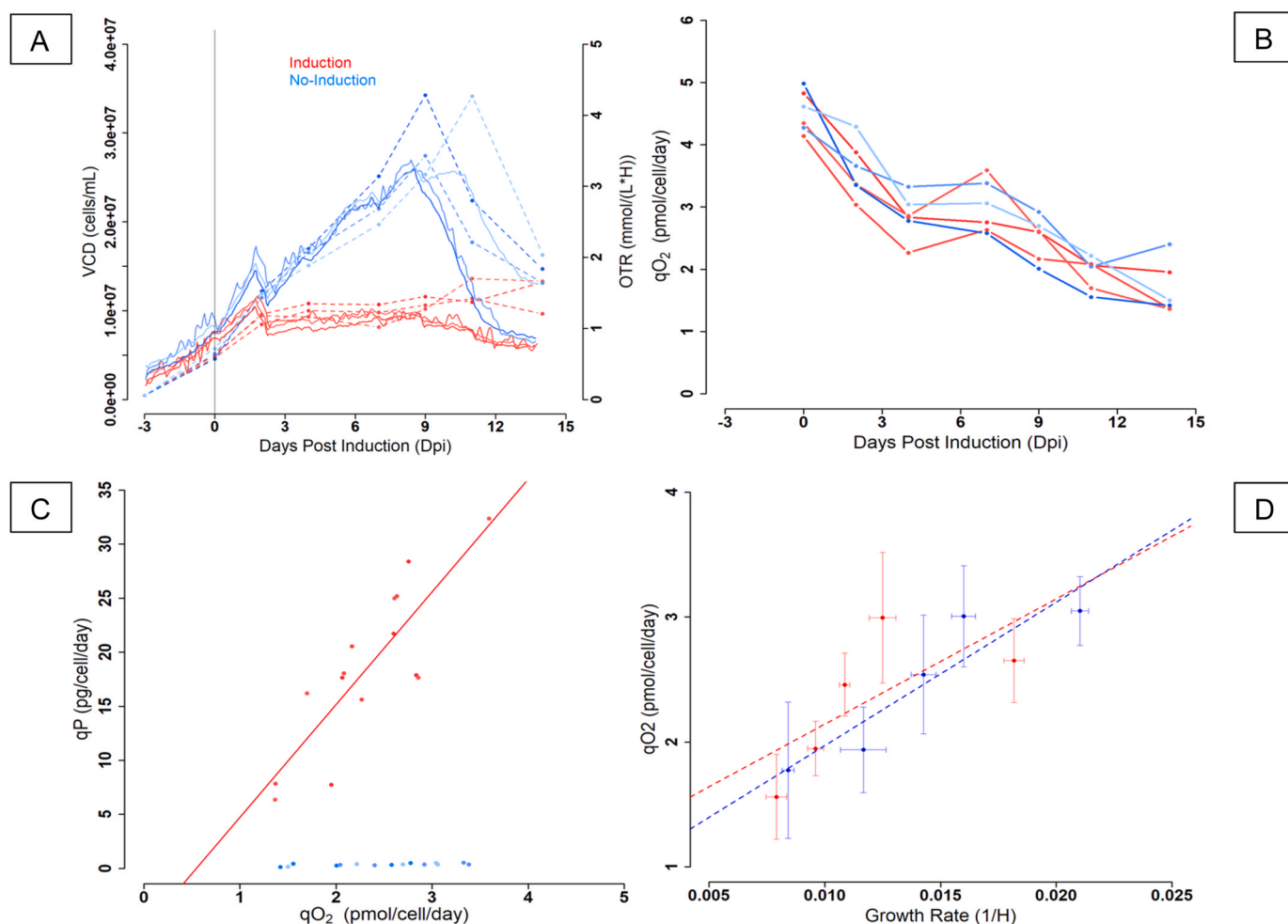
Fig. 3. Impact of induction on A) VCD (dashed lines) and OTR profile (plain lines), B) Specific oxygen respiration rates (qO_2), C) qO_2 vs qP relationship, D) Cell Specific Growth Rate vs qO_2. Two cell culture conditions were studied (induction vs no induction) in triplicate. Three cultures (Induction) were subjected to cumate induction at 0 dpi (day 3) while 3 others were left without induction (No induction condition). A temperature downshift from 37°C to 32°C was performed at 2 dpi (day 5) for both studied conditions. Specific oxygen respiration rates were calculated by taking the nearest OTR value associated to a sampling event and dividing that value by the measured viable cell density.

occurs at 2 dpi (day 5 post-seeding). Higher glycolytic activity is expected in the non-induced condition given the fact that one of the primary functions of glycolysis is to provide relevant building blocks for biosynthesis of NADPH and nucleotides that are important in biomass formation (Lin et al., 2002; Rish et al., 2022). This behaviour is relevant to immortalized cell lines and is denominated Warburg effect (Locasale and Cantley, 2011; Mulukutla et al., 2010; Pereira et al., 2018). Importantly, we observe both high glycolytic activity that is in line with the biomass formation requirements of the non-induced condition, but we also observe lactate consumption activity, suggesting that the cells are undergoing mixed metabolism. This may be explained by the fact that the cell line was selected on the basis of high productivity (Figure 2 SD details a peak cell specific protein productivity of 25–35 pg/cell/day). Given the observed link between lactate re-consumption and high protein productivity (Pereira et al., 2018; Zagari et al., 2013), the cells are able to deploy its efficient lactate metabolism to maintain low concentrations of lactate despite high biosynthesis requirements in the non-induced condition. In Fig. 2D, it is possible to observe the protein production profile of the cultures. Induced cultures reach concentrations of about 2300 mg/L while the non-induced conditions yield concentrations only near 100 mg/L representing a protein production leakage of about 4 %. Most notably, specific protein production is 55-fold higher in induced cultures when compared to non-induced cultures demonstrating how strong of an activator the cumate expression system is.

When evaluating oxygen consumption rates, several trends are detected. In Fig. 3A, it can be discerned how volumetric oxygen consumption can track viable cell density. Notably, one of the non-induced replicates that has delayed cell death (two replicates begin to decline at 9 dpi while in one replicate, the decline occurs at 11 dpi) also has sustained peak OTR until 11 dpi. It can be said that OTR functions as an online early warning predictor of cell growth decline. In the literature, OTR has been shown to have good predictive capacity for viable cell density and viable cell volume as well as cellular viability (Ihling et al., 2021; Ihling, Munkler, Paul, Berg, et al., 2022; Ihling, Munkler, Paul, Lang, et al., 2022; Pappenreiter et al., 2019). Interestingly, it can also be observed that after induction (0 dpi), OTR profiles differ between induced and non-induced conditions. The induced condition exhibits a shortened exponential phase between 0 dpi and 2 dpi (temperature shift from 37°C to 32°C) when compared to its non-induced counterpart. This observation is rather evident when evaluating the OTR plots, but it is hard to determine exclusively from cell counts by 2 dpi. Thus, OTR serves as an important tool to monitor the end of exponential growth which can be critical when formulating time-of-action strategies. This is rather important as previously OTR monitoring was mostly done at the benchtop scale with bioreactors, but with novel monitoring technology at the shake flask scale, it is now possible to multiplex time-of-action characterization studies. Consequently, there exists the potential to save on time and capital expenditures when undertaking exploration of process intensification studies while still relying on reliable physiologically relevant online data. Importantly, the TOM system has been demonstrated to be non-invasive and fully compatible with mammalian cell processes, as no impact on mammalian cell culture kinetics was observed when comparing flasks subjected to OTR measurements with those without OTR measurements (Ihling et al., 2021)(Reyes, Durocher, Schulte, et al., 2022). Furthermore, studies have shown that variations in the dissolved oxygen concentration during the measurement phase of CHO cell cultures are under 1 % of the oxygen saturation concentration, confirming that these variations are negligible compared to the rates of oxygen transfer and consumption in the flask (Ihling et al., 2021). Lastly, as cell free OTR_{max} measurements with the sulfite method indicate that peak maximum OTR for the 250-mL shake flask with 50 mL filling volume is 6.91 ± 0.25 (n = 3) mmol/(L*H). This confirms that the system is never oxygen-limited, as the peak OTR under non-induced conditions remains below this value. Consequently, the dissolved oxygen concentration is never near 0 % saturation (Ihling et al., 2023),

ensuring that any possible variations during the measurement phase do not reach critically low levels.

In Fig. 3B, it is possible to distinguish the specific oxygen respiration rates after induction (0 dpi to 14 dpi). In both induced and non-induced conditions, specific oxygen respiration rates follow the same trend and span the same values. Notably, the estimated specific oxygen respiration rates fall within the range of values reported in literature (Goh et al., 2020; Goudar et al., 2011; Ihling, Munkler, Paul, Berg, et al., 2022). In Fig. 3C, it can be observed that specific oxygen respiration rates and specific protein production rates have a fairly linear relationship ($R^2 = 0.7$) in the induced condition. Such observation has been realized previously in the literature (Zalai et al., 2016). This tight physiological link between protein production rates and specific oxygen respiration rates can be explained by the fact that respiratory activity correlates with high TCA cycle activity (oxidative metabolism) (Nargund et al., 2015; Zagari et al., 2013). In addition, high oxidative metabolism has also been found to correlate with high protein production rates (Templeton et al., 2013). Thus, specific oxygen respiration rates serve as an indirect way to monitor TCA cycle activity and consequently cellular productivity. It is important to note that TCA activity can be influenced by varying nutrient concentrations, which in turn could affect specific respiratory and productive rates. Previous studies have shown that metabolic fluxes are process time-dependent and can be modulated by changes in feed composition (Kirsch et al., 2022; Xu et al., 2023). However, in our study, glucose concentrations never dropped below 5 mmol/L in the non-induced conditions or below 13 mmol/L in the induced conditions throughout the fed-batch culture. This indicates that the increased specific protein productivity observed in the induced conditions was not due to glucose depletion. By 2 dpi, residual glucose concentrations were 18.3 mmol/L on average for the induced condition and 16.9 mmol/L for the non-induced condition, with similar amino acid concentrations across both conditions (Fig. 3S). Despite comparable nutrient levels at this time point, volumetric titer production was significantly higher in the induced condition (128 mg/L) compared to the non-induced condition (0 mg/L). This suggests that the observed differences in productivity were primarily driven by induction effects rather than nutrient limitations or metabolic flux adjustments caused by feed composition. When analysing Fig. 3D, it is evident that increasing growth rates correspond to higher specific oxygen consumption rates, which aligns with existing literature (Muralidharan et al., 2024). As cells proliferate, their demand for oxygen increases to support respiration (Doran, 1995). Therefore, the specific oxygen uptake rate (qO₂) is directly proportional to the specific growth rate. Interestingly, the slopes and intercepts of the regression models for the induced and non-induced conditions are similar. An ANOVA was conducted to assess whether there was a statistically significant interaction between growth rate and condition (induced vs. non-induced) in their effect on oxygen consumption (qO₂). The results revealed that while the growth rate was a statistically significant factor (p-value = 0.012) influencing oxygen consumption, no significant interaction between the conditions was observed. This suggests that, although the magnitude of oxygen consumption is similar in both conditions, the relationship between oxygen consumption and growth rate does not differ significantly between the induced and non-induced groups. This observation may be explained by the fact that a basal amount of oxygen is required to sustain aerobic mammalian cell cultures before oxygen limitation negatively impacts culture outcomes (Fernandes-Platzgummer et al., 2014; Ozturk and Palsson, 1990).

When analysing amino acid concentrations, it is possible to see that asparagine and cystine reach depletion or near depletion levels at different points in time for the non-induced condition (Fig. 4A and Fig. 4B). Asparagine decreases to 0.13 mmol/L by 4 dpi (Fig. 4A) and sustains the low concentrations until 14 dpi at which point the concentration is 0.03 mmol/L. This is despite the fact that the feed supplemented is rich in asparagine (40.17 mmol/L), thus indicating high consumption requirements for both conditions. As it can be observed in Table 3, asparagine consumption rates are high in both conditions
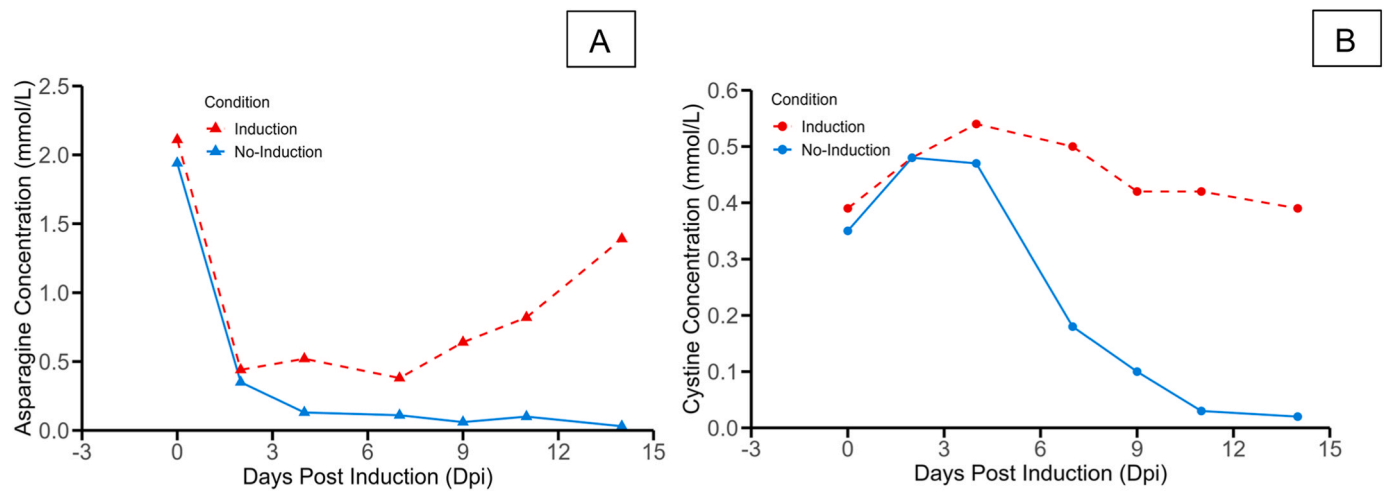
Fig. 4. Impact of induction on A) Asparagine concentration in spent media and B) Cystine concentration in spent media. Induced culture was subjected to cumate induction at 0 dpi (day 3) while no-induction culture was left without induction. A temperature downshift from 37°C to 32°C was performed at 2 dpi (day 5) for both studied conditions.

Table 3
Average cell specific uptake/secretion rates of 20 amino acids (pmol/cell/day) across culture time. Negative sign indicates secretion while positive sign indicates uptake.

	Non-induced cultures	Induced cultures	Fold Change (Induced over non-induced)
His	0.006	0.006	1.0
Asn	0.065	0.101	1.6
Ser	0.048	0.074	1.6
Arg	0.016	0.012	0.7
Gln	−0.006	−0.014	2.5
Gly	0.001	−0.010	13.1
Asp	0.084	0.066	0.8
Glu	0.002	−0.009	4.3
Thr	0.018	0.027	1.5
Ala	−0.021	−0.051	2.5
Pro	0.015	0.020	1.3
Cys	0.004	0.003	0.9
Lys	0.028	0.032	1.2
Tyr	−0.007	−0.020	2.7
Met	0.006	0.005	0.8
Val	0.031	0.034	1.1
Ile	0.017	0.013	0.8
Leu	0.033	0.033	1.0
Phe	0.009	0.009	1.0
Trp	0.004	0.005	1.2

although it is higher in the induced condition. Consequently, it suggests that the depletion of asparagine in the non-induced condition is due to the higher biomass accumulation. It has been observed in the literature that asparagine represents 5 % of the incoming carbon source during the growth phase and is routinely observed to be the most consumed amino acid for growth requirements (Coulet et al., 2022). Since the non-induced cells continue accumulating biomass and consuming glucose at higher specific rates, it makes sense for asparagine to continue being consumed for growth purposes. It is worth noting that after 4 dpi, aspartate concentration drops from 9.68 mmol/L to 3.67 mmol/L at 7 dpi for the non-induced culture. The decreasing trend continues until 14 dpi, at which point, the concentration is 2.42 mmol/L. This drop coincides with asparagine depletion and may indicate that the cultures increased consumption of aspartate as an alternative pathway to sustain metabolic demand. This observation has been made in CHO cells that were subjected to limitation of asparagine during the growth phase (Duarte et al., 2014). Alternatively, cystine reaches a concentration of 0.18 mmol/L by 7 dpi (Fig. 4B) and continues to be depleted until 14 dpi at which time the concentration is very low (0.02 mmol/L). Cystine has

been noted to be consumed during the growth phase (Coulet et al., 2022). It must be noted that the OTR profile indicates a peak near 3 mmol/(L*H) at around 9 dpi which coincides with a peak viable cell density of about 30x10^6 cells/mL (Fig. 3A). This peak OTR may also coincide with the depletion of asparagine and cystine and may indicate that the cells ceded their growth due to nutrient limitations. Importantly, glucose concentration does not decrease below 5 mmol/L for any of the three replicates. Cell free OTR_{max} measurements with the sulfite method indicate that peak maximum OTR for the 250-mL shake flask with 50 mL filling volume is 6.91 ± 0.25 (n = 3) mmol/(L*H). Thus, it can be said that the system is not glucose-limited nor oxygen-limited. However, since the depleted amino acids are known to be consumed during the growth phase (Coulet et al., 2022), it stands to reason that the observed amino acid depletion caused the cessation of growth.

Since residual glucose was kept above 5 mM at all times during sampling points in the non induced condition and above 13 mM in the induced conditions no critically low glucose concentrations, which have been noted to impact growth (Lu et al., 2005), were detected throughout the culture. However, given the fact that supplementation of glucose tracked volumetric glucose consumption. Estimation of glucose concentration after supplementation was evaluated to determine if differences in the upper end of glucose concentrations post supplementation could explain differences in growth. Importantly, it was determined that before divergence occurs in glucose concentration post feeding at 4 dpi (37 mM in non-induced cultures and 32 mM in induced cultures) differences in cellular growth were already evident (1.0E+07 cells/mL in induced cultures and 1.6E+07 cells/mL in non-induced cultures) suggesting that post supplementation glucose concentrations are not to blame for observed differences in growth. Lastly, critically low concentrations in asparagine (4dpi) and cystine (9dpi) in the non-induced conditions appear late in the culture when observable differences in growth were already detectable. The remaining measured amino acids show similar concentrations (Fig. 3S) in the spent media suggesting that nutrient variations in amino acids could not explain observable differences in growth. Thus, divergence in growth profiles can be postulated to be caused by inducing the cells to express recombinant protein.

When analysing cell specific amino acid uptake/secretion rates (Table 3), several observations can be made. On average, the specific rates of amino acid uptake/secretion are larger in magnitude in the induced cultures when compared to the non-induced cultures. This, in part, may explain the lower specific ammonia production rates between 2 dpi to 7 dpi (Figure 2SB). In the literature, it has been observed that cultures at higher cellular concentrations demonstrate comparatively

lower amino acid specific rates (Sheikholeslami et al., 2013a). This is in line with our observations with the caveat that the cultures at higher cell concentrations are not producing recombinant protein. Noteworthy are the differences in specific uptake/secretion rates for glutamine (Gln), glutamate (Glu), glycine (Gly), alanine (Ala), and Tyrosine (Tyr) which show more than a twofold increase in magnitude. Glutamate and glutamine are intimately related in the metabolism of CHO-GS cell lines as glutamate is supplemented in the feed to aid in glutamine synthesis (Fan et al., 2013). There is no glutamine added in the medium and feed. Glutamate can also be synthesized from proline, arginine, histidine, and alanine (Hagrot et al., 2017; Zhang et al., 2016). The increased secretion rates for glutamate (4.3-fold increase) and glutamine (2.5-fold increase) in the induced condition are indicative of higher TCA cycle activity. In fact, the 1.3-fold increase in proline uptake may also point towards increased activity in the induced condition.

Glycine is a product of serine metabolism that fuels the serine-glycine one-carbon (1 C) metabolic pathway (Amelio et al., 2014; Carinhas et al., 2013; Pereira et al., 2018). Furthermore, glycine can also be generated from threonine through threonine dehydrogenase (TDH) and glycine C-acetyltransferase (Amelio et al., 2014). In addition, threonine can also take part in serine-glycine one-carbon (1 C) metabolic pathway directly through glycine cleavage (Amelio et al., 2014). We observe increased cell specific uptake of serine (1.6-fold increase) and threonine (1.5-fold increase) in the induced condition when compared to the non-induced condition as well as increased secretion of glycine (13.1-fold) in the induced condition. Given the inter-relatedness of these three amino acids in the serine-glycine one-carbon metabolic pathway, it can be postulated that this pathway is more active in the induced condition when compared to the non-induced condition. Since the serine-glycine one-carbon pathway is crucial in the synthesis of glutathione (GSH) which is key in controlling oxidative stress (Pereira et al., 2018), the relationships between GSH levels and cell specific productivity of recombinant proteins have been hypothesized (Chevallier, Andersen, et al., 2020; Chevallier, Schoof, et al., 2020; Orellana et al., 2015). It stands to reason that increased activity (cell specific uptake/secretion) in the amino acids related to 1 C units metabolism (e.g. glycine, serine, threonine) may consequently be interpreted as a response to increased oxidative metabolism that is generally associated with high protein production (Templeton et al., 2013). As our experiment centered around the comparison of induction and no-induction, the resulting differences in cell specific productivity were 55-fold further underscoring the need for potential GSH synthesis in managing oxidative stressed caused by increased TCA cycle activity.

During the plateau phase of cell growth, asparagine represents about 8 % of incoming carbon source (Templeton et al., 2013). In fact, it has been determined that multiple TCA cycle intermediates (e.g. citrate, malate, succinate) derive substantial carbon from asparagine catabolism (Dean and Reddy, 2013). It has been delimited as a key nutrient that has to be replenished to avoid rapid depletion (Sellick et al., 2011; Sellick et al., 2015). A recent CHO metabolism review paper has noted that asparagine is significantly consumed during the production phase and the decline phase (Coulet et al., 2022). Furthermore, it has been shown in the literature that induced cells consume asparagine at higher cell specific rates when compared to non-induced cells (Sheikholeslami et al., 2013b). This, in part, may explain why we observe increased cell specific asparagine uptake (1.6-fold) in the induced condition when compared to the non-induced culture.

Alanine is generally observed to accumulate in the extracellular media in the growth, production, and decline phase (Coulet et al., 2022; Rico et al., 2018; Sheikholeslami et al., 2013b). The hypothesis is that alanine secretion into the cell culture helps reduce ammonium toxicity by acting as a nitrogen reservoir (Savizi et al., 2022). It is believed that the biosynthesis of alanine functions as a stress response to the accumulation of metabolic waste (Chitwood et al., 2023). Furthermore, the metabolic link between glutamine and alanine involves the glutamine-pyruvate transaminase reaction. In this process, glutamate is

converted into α-ketoglutarate, and its amine group is transferred to pyruvate to form alanine (Kirsch et al., 2022). These transaminase reactions, such as those involving glutamine-pyruvate and glutamate-aspartate transaminase, enable CHO cells to reduce excess ammonia production. This process likely helps create a more favorable environment for cell culture (Kirsch et al., 2022). Given that higher cell specific rates of ammonia production were observed between 2 dpi to 7 dpi in the induced condition, it stands to reason that the increased cell specific secretion rates of alanine (2.5-fold) are a direct stress response to ammonia accumulation.

Tyrosine is a non-essential amino acid that is known to be consumed during growth for biomass formation (Coulet et al., 2022; Traustason, 2019). In the literature, it has been observed that both induced and non-induced cultures consume tyrosine at equal rates (Sheikholeslami et al., 2013b). We observe cell specific secretion rates in both induced and non-induced conditions. However, the cell specific secretion rate is lower in the non-induced when compared to its induced counterpart (2.7-fold increase in secretion for the induced condition). This may indicate that some of the synthesized tyrosine was re-purposed for biomass growth as the non-induced condition continues growing until 9 dpi (Fig. 3A) while the induced condition secedes growth after 2 dpi (Fig. 3A).

3.2. Time-of-action optimization experiments

Since a metabolic load was observed to be caused by recombinant protein production which decreased growth rates before temperature shift (2 dpi = day 5), it was hypothesized that by recoupling induction and temperature shift, an increase in cell concentration at induction could be obtained. By increasing the cell density at the point of induction, an increase in recombinant protein yield with respect to the previous standard induced condition (induction at day 3 and temperature shift at day 5) may be obtained as well. Thus, the impact of delaying simultaneous induction and temperature downshift to day 5, 6, 7, 9 was evaluated. Feed regimen was kept constant with respect to the previous experiments, but increased sampling was realized to monitor glucose every 2 days eliminating the 3-day weekend schedule and decrease the amount of glucose supplementation that is required in a single sampling day to avoid under or over glucose feeding. As can be seen from Fig. 5A, IVCC is observed to increase by simultaneously delaying induction and temperature shift. However, the gain shows diminishing returns between day-7 and day-9 cultures suggesting that an optimal exists for the given process parameters. From Fig. 5B, it seems that viability can be sustained for 17 days without decreasing below 80 % for any of the conditions. Paradoxically, day-9 induction and temperature shift resulted in the highest endpoint viability (>90 %). However, cell counting aggregation rates reached above 40 % (data not shown) indicating that the reliability of viability estimation may have been impacted by the high cell concentrations. The high endpoint viability in all the tested conditions suggests that the more frequent supplementation of glucose dampened concentration oscillations and thus extended viability in the process when compared to the previous non-induced conditions. In Fig. 5C, a clear view of the viable cell density kinetics can be discerned. The control condition reduced its growth rate after day 3 (induction point) and subsequently temperature shifted on day 5 at a cellular concentration of 10×10^6 cells/mL. By delaying induction just two more days (inducing and temperature shifting at day 5), the process undergoes protein production at 12×10^6 cells/mL. By delaying induction and temperature shift one more day (inducing and temperature shifting at day 6), the process begins protein production at 20×10^6 cells/mL. Furthermore, by delaying one day further (inducing and temperature shifting at day 7), the process undergoes protein production at 25×10^6 cells/mL. Lastly, by delaying two more days (inducing and temperature shifting at day 9) protein production begins at 28×10^6 cells/mL. Given the fact that cells slow down their exponential growth between day 7 and day 9 and noting that the process is not glucose-limited nor oxygen-
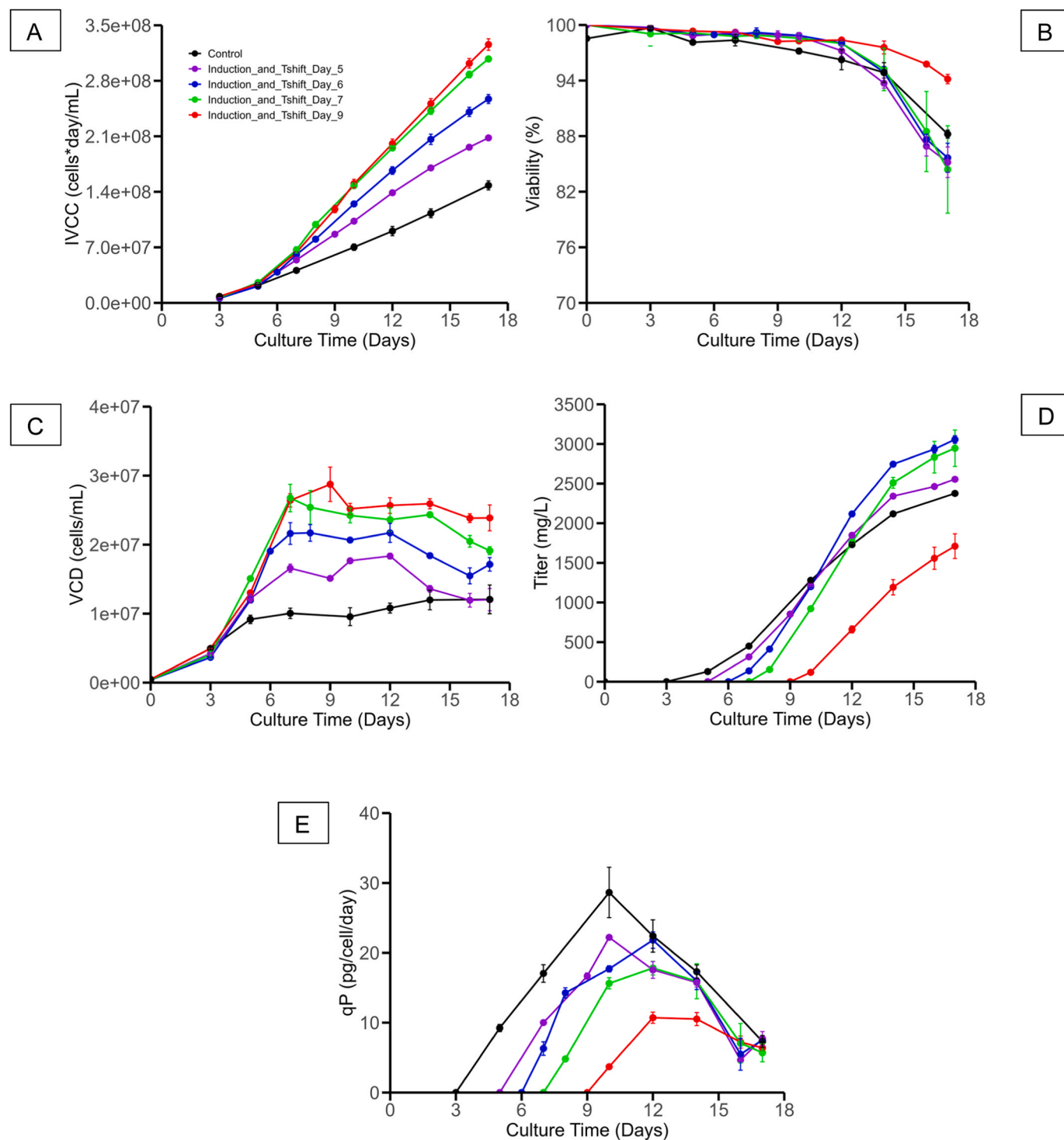
Fig. 5. Impact of time-of-action experimental conditions on A) IVCC, B) Viability, C) Viable cell density (VCD), D) Titer profile, E) Specific protein production profile (qP). Error bars represent standard deviation of 2 replicates. Temperature shift (Tshift) from 37°C to 32°C was realized concomitantly with cumate induction in all conditions except for the control. In the control condition, induction was realized on day 3 and temperature downshift was performed on day 5. Control conditions represent the data of previous induced condition averaged out (3 replicates).

limited, it stands to reason that amino acid depletion may be the culprit with respect to decreased growth. Notably since asparagine and cystine were observed to be depleted in the non-induced condition (Fig. 4), it can be hypothesized that these key amino acids (Coulet et al., 2022; Sellick et al., 2011; Sellick et al., 2015) played a part in limiting biomass accumulation. Furthermore, methionine (Met) was also observed to sustain low concentration values throughout the culture in the

non-induced conditions (Figure 3SB). Given that Met is an essential amino acid and its adequate supplementation is critical avoiding growth limitations (Xing et al., 2011; Xu et al., 2023), it may also be hypothesized to have played a role in growth reduction.

When evaluating Fig. 5D, it can be observed that an optimal zone exists with respect to recombinant protein production yield. Delaying induction and temperature downshift to day 5, 6, and 7 represents a

positive increase in overall therapeutic product concentration specially when compared to induction on day 3 and temperature shifting on day 5 (control condition). In fact, by delaying induction and temperature to day 6 or day 7, a significant increase of 34 % in recombinant protein production (from 2300 mg/L to 3100 mg/L) is obtained which is a significant improvement. In contrast, for the condition of induction and temperature shift at day 9, endpoint protein concentration drops below that of inducing at day 3 and temperature shifting at day 5 reaching just 1500 mg/L. This low performance represents a near 2-fold decrease in therapeutic product concentration with respect to day-6 and day-7 induction/temperature shift. In Fig. 5E, specific protein production rates can be observed to decrease with increasing cellular density at induction and temperature downshift. This phenomenon has been noted previously in inducible cell lines undergoing batch mode operation (Mellahi et al., 2019; Sheikholeslami et al., 2013a). However, the steep decrease in specific productivity on day-9 induction and to a certain extent on day-7 induction may be explained by nutrient depletion. As cystine was observed to be depleted in the non-induced condition and given the fact that cystine limitations in CHO cell cultures have been noted to negatively impact cell specific recombinant protein production (Ali et al., 2019; Ghaffari et al., 2020), it is reasonable to state that similar levels of exhausting of this key amino acid may have hampered recombinant protein production. Consequently, future experiments can center around increasing the supplementation levels of the feed or targeting supplementation of depleted amino acids to increase specific productivity (Zalai et al., 2016).

When observing metabolic profiles, several distinctions can be made. From Fig. 6A, daily volumetric glucose consumption increases during the exponential phase respective to different culture conditions. Broadly, it can be discerned that glucose consumption only decreases once temperature downshift is applied. The control condition (day-3 induction and day-5 temperature downshift) reduces its daily volumetric consumption after day 5 when temperature downshift occurs. Induction and temperature shift concomitantly on day 5 creates a plateau of daily volumetric consumption with slight increase after day 9. Day-6 induction/temperature downshift causes a decrease in daily volumetric glucose consumption. Day-7 induction/temperature downshift induces a subsequent decrease in daily volumetric glucose consumption. Similarly, day-9 induction/temperature shift causes a decrease in daily volumetric glucose consumption. Similar observations with respect to the specific glucose uptake rates can be made (Figure 4SA). Specific glucose uptake rates show reduction after the induction/temperature downshift is realized in each condition.

Lactate switch from production to consumption is a desirable trait in industrial CHO cell cultures (Pereira et al., 2018; Zagari et al., 2013). Several hypothesis and observations have been discussed. Low glucose concentration has been shown to decrease glycolytic flux and consequently lower extracellular lactate concentrations (Konakovsky et al., 2016). Furthermore, reduction in pH setpoint and temperature downshift have also been suggested to induce lactate uptake (Trummer et al., 2006). We observe consistent lactate consumption at around 15 mmol/L (Fig. 6B), regardless of differences in temperature shift and glucose concentration, occurs in an uncontrolled pH environment. In addition, specific lactate rates (Figure 4SB) show no difference between induction/temperature shift points underscoring that the differences in lactate concentration (Fig. 6B) are mainly driven by cell density. This
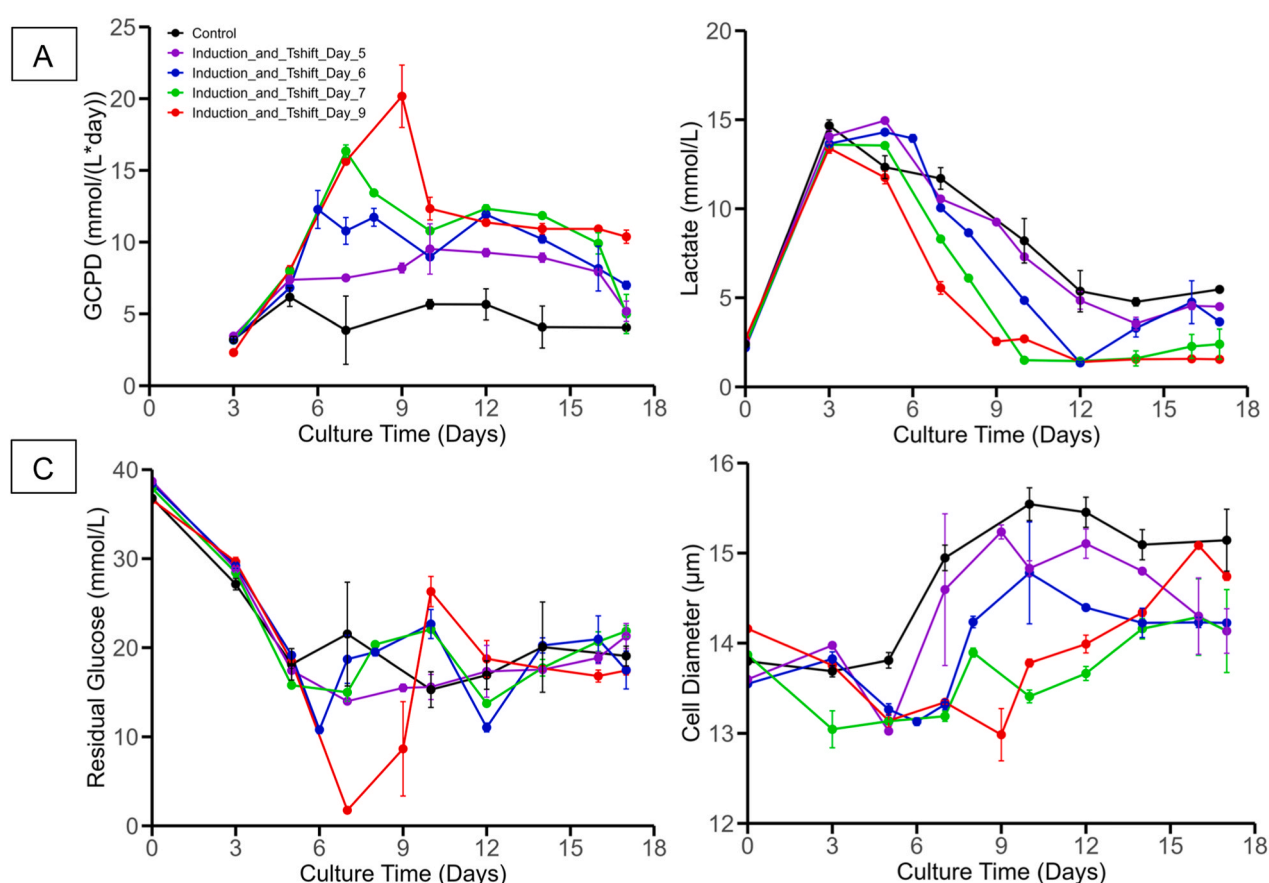

Fig. 6. Impact of time-of-action experimental studies on A) Glucose consumed per day (GCPD), B) Lactate profile, C) Residual glucose, D) Cellular diameter. Error bars represent standard deviation of 2 replicates. Temperature shift (Tshift) from 37°C to 32°C was realized concomitantly with cumate induction in all conditions except control. In the control condition, induction was realized on day 3 and temperature shift was performed on day 5. Control conditions represent the data of previous induced condition averaged out (3 replicates).

suggestion is supported by the observation made with Fig. 6B that the higher the cell density, the lower the lactate concentration. Furthermore, despite divergences in growth rates (Figure 4SC) which would indicate variations in metabolic growth requirements (Lin et al., 2002; Rish et al., 2022), lactate switches to consumption are nonetheless detected. Thus, the mechanism behind lactate consumption may lie in redox balancing of NAD+ /NADH ratios. Initially, a high glycolytic flux leads to an excess production of NADH, resulting in the production of lactate to regenerate NAD+ . When the glycolytic flux decreases, the NADH levels are reduced, altering the NAD+ /NADH ratio (Hartley et al., 2018). This shift causes lactate to be consumed in order to restore the balance (Hartley et al., 2018; Luginsland et al., 2024). Consequently, lactate uptake aids in regulating redox balance and given the fact that redox unbalances negatively impact cellular health (Grüning et al., 2010; Wilkens et al., 2011), it makes sense that clones that fail to adequately regulate their redox state through lactate consumption are associated with reduced titer and growth rates (Pereira et al., 2018; Zagari et al., 2013). Furthermore, since the redox regulation of the cell is related to an interplay between glycolytic activity (down-regulation) and TCA cycle activity (up-regulation), the selection of cell lines on the basis of high oxidative metabolic capacity has been shown to relate to lactate consumption (Luo et al., 2012; Zagari et al., 2013). Given the fact that a strong relationship exists between high oxidative metabolism and specific productivity (Templeton et al., 2013) and also taken in account that the cell line was selected on the basis of its high productive capacity, it is suggested that the lactate consumption observed in the cells irrespective of induction timepoints (or lack there off) and temperature

downshift timepoints is a consequence of its ability to regulate redox potential.

In Fig. 6C, the residual glucose concentration can be distinguished. Broadly, glucose concentrations were controlled around a 10 mmol/L to 25 mmol /L range underscoring the importance of increased sampling frequency for glucose monitoring at high cell densities. However, in the day-9 induction/temperature downshift condition, residual glucose concentrations reached near depletion levels (1.5 mmol/L). Subsequent glucose supplementation restored nutrient levels above the depletion range, and given the glucose consumed profile, glycolytic activity returned to normalcy (approx. 25 mmol/L) then decreased on day 10. Fig. 6D shows that the increase in cellular diameter is driven mainly by changes in temperature ($37°C$ to $32°C$) rather than recombinant protein production. In the control condition (day-3 induction and day-5 temperature shift), cell diameter increases after temperature shift occurred on day 5 even though onset of recombinant protein production began on day 3. In contrast, cell diameter increases on the day of the two simultaneous actions (induction and temperature downshift) for the 3 other studied conditions. As noted previously, temperature-related impact on cell diameter has been detected in CHO cells (Martínez et al., 2015; Tait et al., 2013) and associated to G1 phase cell cycle arrest (Pan et al., 2017) (Jing-Xiu et al., 2004).

By analyzing OTR profiles (Fig. 7A), several trends can be noted. As shown previously (Fig. 1B), the onset of recombinant protein production underscores an increased metabolic load that reduces the growth rate of the cultures before temperature shift is realized to induce cell cycle arrest. Non-induced cells continue their exponential growth up until
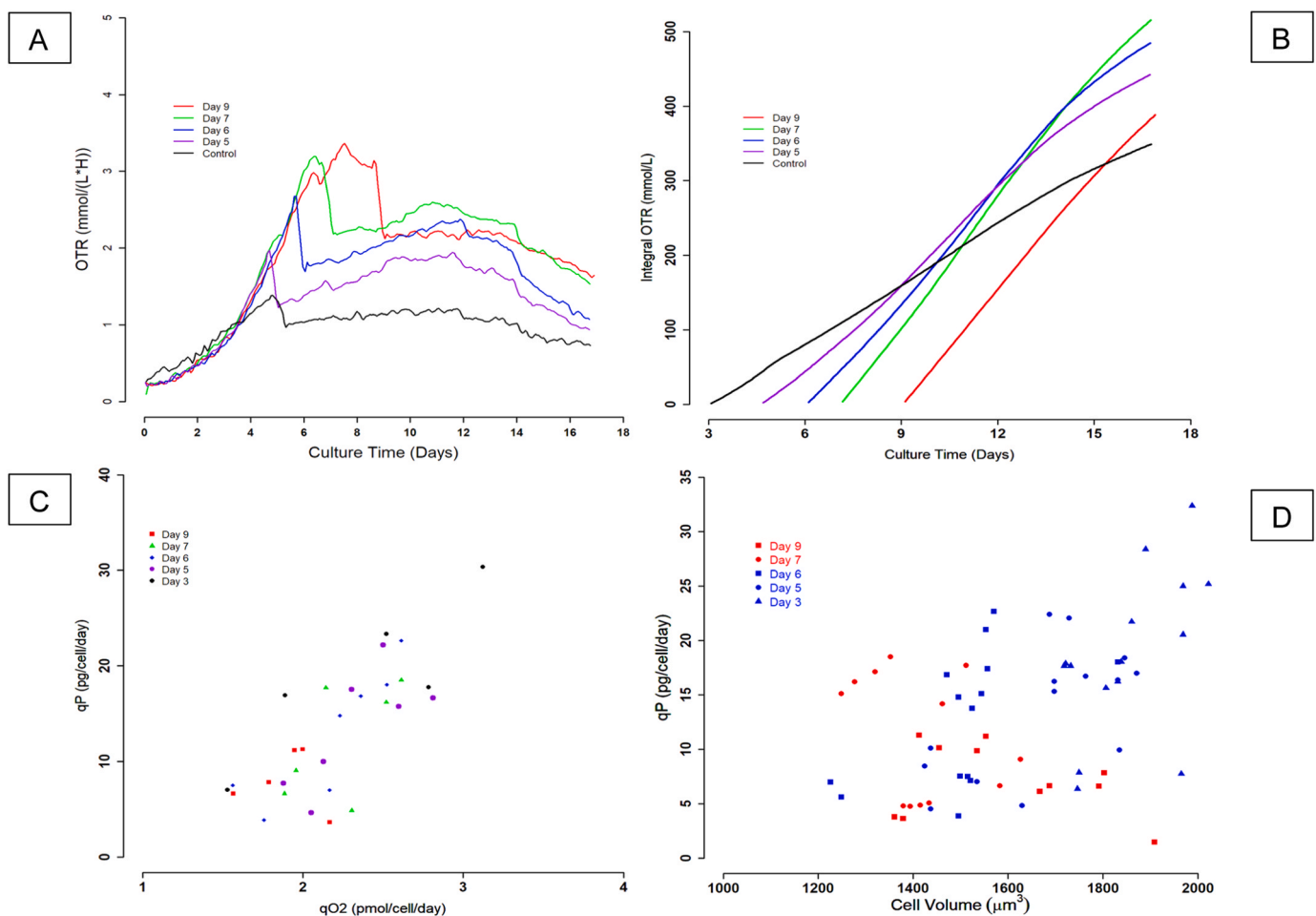
Fig. 7. Impact of time-of-action studies on A) OTR profile, B) Integral of OTR, C) Cell specific oxygen respiration rate (qO_2) and cell specific protein productivity (qP) relationship, D) Cell specific protein productivity (qP) and cell volume relationship.

induction and temperature shift. However, it can be observed that day-9 induction/temperature shift is taken out of the exponential phase by day 6 and in fact reduces its OTR value by day 7. This change in the OTR profile can be explained by the fact that residual glucose reached near depletion levels (1.5 mmol/L) on day 7 (Fig. 6C), probably impacting its ability to sustain high glycolytic activity that is required for biomass accumulation (Locasale and Cantley, 2011; Mulukutla et al., 2010; Pereira et al., 2018). Decreases in OTR profiles caused by the depletion of carbon sources have been noted previously (Ihling et al., 2021; Ihling et al., 2022). OTR profile increased once glucose levels were brought above depletion but a subsequent plateau near 3 mmol/(L*H) was reached. This plateau holds a similar resemblance to the one observed in the non-induced condition (Fig. 3A). Given the fact that asparagine and cystine were observed to reach depletion levels in the non-induced condition (Fig. 4), it can be assumed that the observed plateau in the OTR profile is a direct consequence of asparagine and cystine limitations that are known to impact cell growth (Coulet et al., 2022; Duarte et al., 2014). In the literature, amino acid related limitations have also been detected through careful analysis of OTR profiles (Zalai et al., 2016). Furthermore, OTR profiles start decreasing after day 14 which coincides with a decrease in viability (Fig. 5B). Notable decreases in OTR profiles that coincide with onset of viability decline have been noted in the literature (Gálvez et al., 2012; Lecina et al., 2006). In fact, this reduction in OTR has been suggested as a point of harvest (Lecina et al., 2022). Interestingly, cell specific oxygen respiration rates retain similar trends across all conditions (Fig. 4 SD). This was expected as specific oxygen respiration rates were similar between induced and non-induced conditions (Fig. 3B). Notably, increased feed supplementation on day 6 induction culture conditions showed no notable benefit on cell growth and volumetric titer (Fig. 5S) while increased culture time (from day 17 to day 19) showed no benefit on titer accumulation (Fig. 5S).

As can be seen in Fig. 7A (day 3–5) induction at 37°C causes the rate of OTR increase to slow down when compared to not inducing at 37°C. Given the interrelationship between viable biomass and OTR it can be expected that the observed difference in increases of OTR also relates to differences in cell growth. Thus, inducing at 37°C diminishes possible growth while also not benefiting from productivity gains observed with temperature shifts in the wider literature (Bedoya-López et al., 2016; Xu et al., 2019; Zhu et al., 2023). Consequently, implementing a 32°C temperature shift post-induction is crucial for balancing cell growth and productivity, and optimizing the timing of this shift can maximize titer gains.

In Fig. 7B, the integral of the OTR curves post-induction can be evaluated. When analyzed alongside the titer profiles (Fig. 5D), it can be visualized that a similar ranking in descending order (from highest protein yield to lowest protein yield) can be obtained. The two conditions (day-6 and day-7 induction/temperature shift) that produced the most volumetric amount of protein are also the two conditions that have the highest area under the curve post-induction. Furthermore, day-5 induction/temperature shift that had a protein production higher than day-3 induction but less than day-6 and day-7 induction is also ranked accordingly. However, day-9 induction which had less protein production than day-3 induction (control) is ranked higher in the OTR integral plot. It must be stressed that this culture most likely suffered cystine depletion given that the previous non-induced condition that reached high biomass values encountered cystine depletion by day 10 of the culture (Fig. 4B). Furthermore, cystine depletion is known to severely impact cell specific productivity of recombinant protein (Ali et al., 2019; Ghaffari et al., 2020). Consequently, it stands to reason that with adequate supplementation of exhausted amino acids, specific productivity can be increased to levels like the ones attained in the day-7 induction/temperature shift condition. Improved protein outcomes above the standard day-3 induction condition but below day-7 and day-6 induction/temperature shift can be expected given the fact that the length of time available for protein production before viability reduction is comparatively less. In conclusion, it can be said that the

integral of OTR is a relevant parameter to monitor as a qualitative soft sensor of recombinant protein production. This postulate has physiological basis on the fact that respiratory activity correlates with high TCA cycle activity (Nargund et al., 2015; Zagari et al., 2013) and in turn, high TCA cycle activity strongly correlates with high protein production (Templeton et al., 2013). In Fig. 7C, this tight physiological link can be seen at play. Broadly, post-induction cell specific oxygen respiratory rates retain a linear relationship with cell specific protein production rates. Higher cell specific oxygen respiration rates in the day-3 induction condition also correlate with proportionally higher cell specific productivity. Furthermore, the day-9 induction/temperature shift condition had a lower cell specific productivity and consequently also had comparatively lower cell specific oxygen respiration rates during the production phase. Similar relationships between cell specific oxygen respiration rates and cell specific productivity have also been noted (Zalai et al., 2016). Lastly, in Fig. 7D, a scatter plot showing the relationship between cell volume and specific productivity can be seen. As cellular volume increases, specific cellular productivity also increases for induction conditions on day 3, day 5, and day 6. This phenomenon has been noted previously in other mammalian cell cultures (Huang et al., 2010; Wang et al., 2024). As noted previously, it has been discovered that the increase in cell volume is associated with enhanced transcription, translation, and secretion machinery. Given the fact that temperature downshifting triggers a coordinated response that affects the cell cycle, transcription, and translation processes (Kumar et al., 2007) and given the observation that decreases in temperature can enhance cell-specific productivity by stabilizing mRNAs, increasing transcription levels, and improving protein folding (Shahabi et al., 2023), it can be suggested that the observed correlation between specific productivity and cell volume (Edros et al., 2014; Khoo and Al-Rubeai, 2009) is a result of an indirect relationship between specific productivity and enhanced transcription and translation levels. Changes in temperature cascade result in changes in transcription, cell cycle, and cellular machinery that are beneficial to recombinant protein production but are not unique to recombinant protein production. Day-9 induction/temperature shift does not sustain this relationship. Similarly, in day-7 induction/temperature shift, cellular volume continues to increase while cell specific productivity plateaus and trends downwards after day 14.

4. Conclusions

OTR monitoring has allowed us to identify key process related impacts such as the metabolic load that recombinant protein expression exerts on CHO cell cultures causing a diminishing growth rate. Increased cell specific glucose consumption was observed in the non-induced conditions indicating higher glycolytic activity in the absence of recombinant protein production pressure, which is coherent with the increased biomass accumulation. In addition, observed reduction in cell specific ammonia secretion rates in the non-induced condition hints at decreased amino acid catabolism. Furthermore, cell specific amino acid uptake/secretion rates demonstrated increased activity in the induced conditions when compared to non-induced conditions which is inline with expectations of higher TCA cycle activity during recombinant protein production. Interestingly, cell specific oxygen respiratory rates were demonstrated to hold a tight relationship with cell specific recombinant protein production which aligns with literature reports of oxidative metabolism and recombinant protein expression. Thanks to careful metabolic analysis of the fed-batch process, time-of-action experiments were formulated to optimize the biphasic nature of inducible systems such as increasing biomass accumulation during the growth phase and increasing recombinant protein synthesis during the production phase. By sidestepping the growth limitations that induction conveys on biomass accumulation before temperature shift, gains in volumetric protein production were achieved. A significant increase, 34 %, in endpoint yield within an equal time frame was attained. In

addition, OTR profiles displayed indications of glucose exhaustion before analytical measurements allowed for glucose supplementation on time.

In summary, it can be concluded that online monitoring within shake flasks allows for careful formulation of process intensification strategies in a high-throughput manner. To our knowledge, this is the first report on the implementation of the TOM device to rapidly study the metabolic load of an inducible expression system conveyed to CHO cells at the stage of shake flask development. This innovative approach also allows for early process fingerprinting in which characterization of nutrient-related limitations and identification of adequate points of action such as time of induction and temperature downshift to fast-track process optimization are possible. Further studies to scale up the proposed framework of oxygen consumption-based time of induction into stirred tank bioreactors need to be explored.

Funding information

CRediT authorship contribution statement

Olivier Henry: Writing – review & editing, Supervision, Resources, Funding acquisition, Conceptualization. **Lucas Lemire:** Investigation, Formal analysis, Data curation. **Sebastian-Juan Reyes:** Writing – original draft, Validation, Methodology, Investigation, Data curation, Conceptualization. **Phuong Lan Pham:** Writing – review & editing, Supervision, Resources, Funding acquisition, Conceptualization. **Yves Durocher:** Writing – review & editing, Supervision, Resources, Funding acquisition. **Robert Voyer:** Supervision, Resources, Writing – review & editing.

Declaration of Competing Interest

The authors declare the following financial interests/personal relationships which may be considered as potential competing interests: Olivier Henry reports financial support was provided by Natural Sciences and Engineering Research Council of Canada. If there are other authors, they declare that they have no known competing financial interests or personal relationships that could have appeared to influence the work reported in this paper.

Acknowledgments

Appendix A. Supporting information

Supplementary data associated with this article can be found in the online version at doi:10.1016/j.jbiotec.2025.01.008.

Data availability

Data will be made available on request.

References

Ali, A.S., Raju, R., Kshirsagar, R., Ivanov, A.R., Gilbert, A., Zang, L., Karger, B.L., 2019. Multi-omics study on the impact of cysteine feed level on cell viability and mAb production in a CHO bioprocess. Biotechnol. J. 14 (4), 1800352.

Amelio, I., Cutruzzolá, F., Antonov, A., Agostini, M., Melino, G., 2014. Serine and glycine metabolism in cancer. Trends Biochem. Sci. 39 (4), 191–198.

Anderlei, T., Büchs, J., 2001. Device for sterile online measurement of the oxygen transfer rate in shaking flasks. Biochem. Eng. J. 7 (2), 157–162.

Anderlei, T., Zang, W., Papaspyrou, M., Büchs, J., 2004. Online respiration activity measurement (OTR, CTR, RQ) in shake flasks. Biochem. Eng. J. 17 (3), 187–194.

Bedoya-López, A., Estrada, K., Sanchez-Flores, A., Ramírez, O.T., Altamirano, C., Segovia, L., Valdez-Cruz, N.A.J.P., 2016. Effect of temperature downshift on the transcriptomic responses of Chinese hamster ovary cells using recombinant human tissue plasminogen activator production culture, 11 (3), e0151529.

Carinhas, N., Duarte, T.M., Barreiro, L.C., Carrondo, M.J.T., Alves, P.M., Teixeira, A.P., 2013. Metabolic signatures of GS-CHO cell clones associated with butyrate treatment and culture phase transition. Biotechnol. Bioeng. 110 (12), 3244–3257. https://doi.org/10.1002/bit.24983.

Casablancas, A., Gámez, X., Lecina, M., Solà, C., Cairó, J.J., Gòdia, F., 2013. Comparison of control strategies for fed-batch culture of hybridoma cells based on on-line monitoring of oxygen uptake rate, optical cell density and glucose concentration. Journal of Chemical Technology Biotechnology 88 (9), 1680–1689.

Chevallier, V., Andersen, M.R., Malphettes, L., 2020. Oxidative stress-alleviating strategies to improve recombinant protein production in CHO cells. Biotechnol. Bioeng. 117 (4), 1172–1186.

Chevallier, V., Schoof, E.M., Malphettes, L., Andersen, M.R., Workman, C.T., 2020. Characterization of glutathione proteome in CHO cells and its relationship with productivity and cholesterol synthesis. Biotechnol. Bioeng. 117 (11), 3448–3458.

Chitwood, D.G., Uy, L., Fu, W., Klaubert, S.R., Harcum, S.W., Saski, C.A., 2023. Dynamics of amino acid metabolism, gene expression, and circulomics in a recombinant chinese hamster ovary cell line adapted to moderate and high levels of extracellular lactate. Genes 14 (8), 1576.

Coulet, M., Kepp, O., Kroemer, G., Basmaciogullari, S., 2022. Metabolic profiling of CHO cells during the production of biotherapeutics. Cells 11 (12). https://doi.org/10.3390/cells11121929.

Dean, J., Reddy, P., 2013. Metabolic analysis of antibody producing CHO cells in fed-batch production. Biotechnol. Bioeng. 110 (6), 1735–1747. https://doi.org/10.1002/bit.24826.

Dinger, R., Lattermann, C., Flitsch, D., Fischer, J.P., Kosfeld, U., Büchs, J., 2022. Device for respiration activity measurement enables the determination of oxygen transfer rates of microbial cultures in shaken 96-deepwell microtiter plates. Biotechnol. Bioeng. 119 (3), 881–894.

Doran, P.M., 1995. Bioprocess engineering principles. Elsevier.

Dreesen, I.A., Fussenegger, M., 2011. Ectopic expression of human mTOR increases viability, robustness, cell size, proliferation, and antibody production of chinese hamster ovary cells. Biotechnol. Bioeng. 108 (4), 853–866. https://doi.org/10.1002/bit.22990.

Duarte, T.M., Carinhas, N., Barreiro, L.C., Carrondo, M.J., Alves, P.M., Teixeira, A.P., 2014. Metabolic responses of CHO cells to limitation of key amino acids. Biotechnol. Bioeng. 111 (10), 2095–2106.

Ducommun, P., Ruffieux, P.-A., Furter, M.-P., Marison, I., von Stockar, U., 2000. A new method for on-line measurement of the volumetric oxygen uptake rate in membrane aerated animal cell cultures. J. Biotechnol. 78 (2), 139–147.

Edros, R., McDonnell, S., Al-Rubeai, M., 2014. The relationship between mTOR signalling pathway and recombinant antibody productivity in CHO cell lines. BMC Biotechnol. 14, 1–10.

Elmore, S.J., 2007. Apoptosis: a review of programmed cell death. T. p. 35 (4), 495–516.

Europa, A.F., Gambhir, A., Fu, P.C., Hu, W.S., 2000. Multiple steady states with distinct cellular metabolism in continuous culture of mammalian cells. Biotechnol. Bioeng. 67 (1), 25–34.

Fan, L., Frye, C.C., Racher, A.J., 2013. The use of glutamine synthetase as a selection marker: recent advances in Chinese hamster ovary cell line generation processes. Pharm. Bioprocess. 1 (5), 487–502.

Fernandes-Platzgummer, A., Diogo, M.M., da Silva, C.L., Cabral, J.M., 2014. Maximizing mouse embryonic stem cell production in a stirred tank reactor by controlling dissolved oxygen concentration and continuous perfusion operation. Biochem. Eng. J. 82, 81–90.

Fontova, A., Lecina, M., López-Repullo, J., Martínez-Monge, I., Comas, P., Bragós, R., Cairó, J.J., 2018. A simplified implementation of the stationary liquid mass balance method for on-line OUR monitoring in animal cell cultures. Journal of Chemical Technology Biotechnology 93 (6), 1757–1766.

Gaillet, B., Gilbert, R., Broussau, S., Pilotte, A., Malenfant, F., Mullick, A., Massie, B., 2010. High-level recombinant protein production in CHO cells using lentiviral vectors and the cumate gene-switch. Biotechnol. Bioeng. 106 (2), 203–215. https://doi.org/10.1002/bit.22698.

Gálvez, J., Lecina, M., Solà, C., Cairó, J., Gòdia, F., 2012. Optimization of HEK-293S cell cultures for the production of adenoviral vectors in bioreactors using on-line OUR measurements. J. Biotechnol. 157 (1), 214–222.

Ghaffari, N., Jardon, M.A., Krahn, N., Butler, M., Kennard, M., Turner, R.F., Piret, J.M., 2020. Effects of cysteine, asparagine, or glutamine limitations in Chinese hamster ovary cell batch and fed-batch cultures. Biotechnol. Prog. 36 (2), e2946.

Giese, H., Azizan, A., Kümmel, A., Liao, A., Peter, C.P., Fonseca, J.A., Büchs, J., 2014. Liquid films on shake flask walls explain increasing maximum oxygen transfer capacities with elevating viscosity. Biotechnol. Bioeng. 111 (2), 295–308.

Goh, H.-Y., Sulu, M., Alosert, H., Lewis, G.L., Josland, G.D., Merriman, D.E., 2020. Applications of off-gas mass spectrometry in fed-batch mammalian cell culture. Bioprocess Biosyst. Eng. 43, 483–493.

Goldrick, S., Lee, K., Spencer, C., Holmes, W., Kuiper, M., Turner, R., Farid, S.S., 2018. On-line control of glucose concentration in high-yielding mammalian cell cultures enabled through oxygen transfer rate measurements. Biotechnol. J. 13 (4), e1700607. https://doi.org/10.1002/biot.201700607.

Goudar, C.T., Piret, J.M., Konstantinov, K.B., 2011. Estimating cell specific oxygen uptake and carbon dioxide production rates for mammalian cells in perfusion culture. Biotechnol. Prog. 27 (5), 1347–1357.

Grüning, N.-M., Lehrach, H., Ralser, M., 2010. Regulatory crosstalk of the metabolic network. Trends Biochem. Sci. 35 (4), 220–227.

Guez, J.-S., Müller, C., Danze, P., Büchs, J., Jacques, P., 2008. Respiration activity monitoring system (RAMOS), an efficient tool to study the influence of the oxygen transfer rate on the synthesis of lipopeptide by Bacillus subtilis ATCC6633. J. Biotechnol. 134 (1-2), 121–126.

Hagrot, E., Oddsdóttir, H.Æ., Hosta, J.G., Jacobsen, E.W., Chotteau, V., 2017. Poly-pathway model, a novel approach to simulate multiple metabolic states by reaction network-based model–application to amino acid depletion in CHO cell culture. J. Biotechnol. 259, 235–247.

Hansen, S., Hariskos, I., Luchterhand, B., Büchs, J., 2012. Development of a modified respiration activity monitoring system for accurate and highly resolved measurement of respiration activity in shake flask fermentations. J. Biol. Eng. 6, 1–12.

Hartley, F., Walker, T., Chung, V., Morten, K., 2018. Mechanisms driving the lactate switch in Chinese hamster ovary cells. Biotechnol. Bioeng. 115 (8), 1890–1903. https://doi.org/10.1002/bit.26603.

He, C., Ye, P., Wang, H., Liu, X., Li, F., 2019. A systematic mass-transfer modeling approach for mammalian cell culture bioreactor scale-up. Biochem. Eng. J. 141, 173–181.

Hoshan, L., Jiang, R., Moroney, J., Bui, A., Zhang, X., Hang, T.C., Xu, S., 2019. Effective bioreactor pH control using only sparging gases. Biotechnol. Prog. 35 (1), e2743.

Huang, Y.M., Hu, W., Rustandi, E., Chang, K., Yusuf-Makagiansar, H., Ryll, T., 2010. Maximizing productivity of CHO cell-based fed-batch culture using chemically defined media conditions and typical manufacturing equipment. Biotechnol. Prog. 26 (5), 1400–1410.

Ihling, N., Berg, C., Paul, R., Munkler, L.P., Mäkinen, M.E.L., Chotteau, V., Büchs, J., 2023. Scale-down of CHO cell cultivation from shake flasks based on oxygen mass transfer allows application of parallelized, non-invasive, and time-resolved monitoring of the oxygen transfer rate in 48-well microtiter plates. Biotechnol. J. 18 (11), 2300053.

Ihling, N., Munkler, L.P., Berg, C., Reichenbächer, B., Wirth, J., Lang, D., Büchs, J., 2021. Time-resolved monitoring of the oxygen transfer rate of chinese hamster ovary cells provides insights into culture behavior in shake flasks. Front. Bioeng. Biotechnol. 9, 725498.

Ihling, N., Munkler, L.P., Paul, R., Berg, C., 2022. Introducing oxygen transfer rate measurements as a novel method for time-resolved cytotoxicity assessment in shake flasks. Environ. Sci. Eur. 34 (1), 97.

Ihling, N., Munkler, L.P., Paul, R., Berg, C., Reichenbächer, B., Kadisch, M., Büchs, J., 2022. Non-invasive and time-resolved measurement of the respiration activity of Chinese hamster ovary cells enables prediction of key culture parameters in shake flasks. Biotechnol. J. 17 (8), 2100077.

Jing-Xiu, B., Shuttleworth, J., Al-Rubeai, M., 2004. Uncoupling of cell growth and proliferation results in enhancement of productivity. Biotechnol. Bioeng. 85 (7), 741–749.

Joubert, S., Stuible, M., Lord-Dufour, S., Lamoureux, L., Vaillancourt, F., Perret, S., Durocher, Y., 2023. A CHO stable pool production platform for rapid clinical development of trimeric SARS-CoV-2 spike subunit vaccine antigens. Biotechnol. Bioeng. 120 (7), 1746–1761. https://doi.org/10.1002/bit.28387.

Joubert, S., Stuible, M., Lord-Dufour, S., Lamoureux, L., Vaillancourt, F., Perret, S., Mahimkar, R., 2023. A CHO stable pool production platform for rapid clinical development of trimeric SARS-CoV-2 spike subunit vaccine antigens. Biotechnol. Bioeng. 120 (7), 1746–1761.

Kafri, M., Metzl-Raz, E., Jona, G., Barkai, N., 2016. The cost of protein production. Cell Rep. 14 (1), 22–31.

Khoo, S.H.G., Al-Rubeai, M., 2009. Detailed understanding of enhanced specific antibody productivity in NS0 myeloma cells. Biotechnol. Bioeng. 102 (1), 188–199.

Kim, T.K., Chung, J.Y., Sung, Y.H., Lee, G.M., 2001. Relationship between cell size and specific thrombopoietin productivity in Chinese hamster ovary cells during dihydrofolate reductase-mediated gene amplification. Biotechnol. Bioprocess Eng. 6, 332–336.

Kirsch, B.J., Bennun, S.V., Mendez, A., Johnson, A.S., Wang, H., Qiu, H., Betenbaugh, M. J., 2022. Metabolic analysis of the asparagine and glutamine dynamics in an industrial Chinese hamster ovary fed-batch process. Biotechnol. Bioeng. 119 (3), 807–819. https://doi.org/10.1002/bit.27993.

Klöckner, W., Gacem, R., Anderlei, T., Raven, N., Schillberg, S., Lattermann, C., Büchs, J., 2013. Correlation between mass transfer coefficient k L a and relevant operating parameters in cylindrical disposable shaken bioreactors on a bench-to-pilot scale. J. Biol. Eng. 7, 1–14.

Konakovsky, V., Clemens, C., Müller, M.M., Bechmann, J., Berger, M., Schlatter, S., Herwig, C., 2016. Metabolic control in mammalian fed-batch cell cultures for reduced lactic acid accumulation and improved process robustness. Bioengineering 3 (1), 5.

Koscielny, A., Liszewska, E., Machnicka, K., Wezyk, M., Kotulska, K., Jaworski, J., 2021. mTOR controls endoplasmic reticulum–golgi apparatus trafficking of VSVg in

specific cell types. Cell. Mol. Biol. Lett. 26 (1), 18. https://doi.org/10.1186/s11658-021-00262-z.

Kumar, N., Gammell, P., Clynes, M., 2007. Proliferation control strategies to improve productivity and survival during CHO based production culture: a summary of recent methods employed and the effects of proliferation control in product secreting CHO cell lines. Cytotechnology 53, 33–46.

Kussow, C.M., Zhou, W., Gryte, D.M., Hu, W.-S., 1995. Monitoring of mammalian cell growth and virus production process using on-line oxygen uptake rate measurement. Enzym. Microb. Technol. 17 (9), 779–783.

Lecina, M., Comas, P., Martínez-Monge, I., Cairó, J.J., 2022. Monitoring tools for the development of high cell density culture strategies. Cell Culture Engineering and Technology: In appreciation to Professor Mohamed Al-Rubeai. Springer, pp. 485–510.

Lecina, M., Soley, A., Gràcia, J., Espunya, E., Lázaro, B., Cairó, J., Gòdia, F., 2006. Application of on-line OUR measurements to detect actions points to improve baculovirus-insect cell cultures in bioreactors. J. Biotechnol. 125 (3), 385–394.

Li, Z., Rinas, U., 2020. Recombinant protein production associated growth inhibition results mainly from transcription and not from translation. Microb. Cell Factor. 19, 1–11.

Lin, J., Takagi, M., Qu, Y., Yoshida, T., 2002. Possible strategy for on-line monitoring and control of hybridoma cell culture. Biochem. Eng. J. 11 (2), 205–209. https://doi.org/10.1016/S1369-703X(02)00028-1.

Lloyd, D.R., Holmes, P., Jackson, L.P., Emery, A.N., Al-Rubeai, M., 2000. Relationship between cell size, cell cycle and specific recombinant protein productivity. Cytotechnology 34 (1-2), 59–70. https://doi.org/10.1023/a:1008103730027.

Locasale, J.W., Cantley, L.C., 2011. Metabolic flux and the regulation of mammalian cell growth. Cell Metab. 14 (4), 443–451. https://doi.org/10.1016/j.cmet.2011.07.014.

Losen, M., Frölich, B., Pohl, M., Büchs, J., 2004. Effect of oxygen limitation and medium composition on Escherichia coli fermentation in shake-flask cultures. Biotechnol. Prog. 20 (4), 1062–1068.

Lu, S., Sun, X., Zhang, Y., 2005. Insight into metabolism of CHO cells at low glucose concentration on the basis of the determination of intracellular metabolites. Process Biochem. 40 (5), 1917–1921. https://doi.org/10.1016/j.procbio.2004.07.004.

Luginsland, M., Kontoravdi, C., Racher, A., Jaques, C., Kiparissides, A., 2024. Elucidating lactate metabolism in industrial CHO cultures through the combined use of flux balance and principal component analyses. Biochem. Eng. J. 202, 109184.

Luo, J., Vijayasankaran, N., Autsen, J., Santuray, R., Hudson, T., Amanullah, A., Li, F., 2012. Comparative metabolite analysis to understand lactate metabolism shift in Chinese hamster ovary cell culture process. Biotechnol. Bioeng. 109 (1), 146–156.

Maier, U., Büchs, J., 2001. Characterisation of the gas–liquid mass transfer in shaking bioreactors. Biochem. Eng. J. 7 (2), 99–106.

Maier, U., Losen, M., Büchs, J., 2004. Advances in understanding and modeling the gas–liquid mass transfer in shake flasks. Biochem. Eng. J. 17 (3), 155–167.

Maltais, J.-S., Lord-Dufour, S., Morasse, A., Stuible, M., Loignon, M., Durocher, Y., 2023. Repressing expression of difficult-to-express recombinant proteins during the selection process increases productivity of CHO stable pools, 120 (10), 2840–2852. https://doi.org/10.1002/bit.28435.

Mancilla, E., Palacios-Morales, C., Córdova-Aguilar, M., Trujillo-Roldán, M., Ascanio, G., Zenit, R., 2015. A hydrodynamic description of the flow behavior in shaken flasks. Biochem. Eng. J. 99, 61–66.

Martínez, V.S., Buchsteiner, M., Gray, P., Nielsen, L.K., Quek, L.-E., 2015. Dynamic metabolic flux analysis using B-splines to study the effects of temperature shift on CHO cell metabolism. Metab. Eng. Commun. 2, 46–57.

Martínez-Monge, I., Comas, P., Triquell, J., Lecina, M., Casablancas, A., Cairó, J., 2018. A new strategy for fed-batch process control of HEK293 cell cultures based on alkali buffer addition monitoring: comparison with OUR dynamic method. Appl. Microbiol. Biotechnol. 102, 10469–10483.

Martínez-Monge, I., Roman, R., Comas, P., Fontova, A., Lecina, M., Casablancas, A., Cairó, J., 2019. New developments in online OUR monitoring and its application to animal cell cultures. Appl. Microbiol. Biotechnol. 103, 6903–6917.

McVey, D., Aronov, M., Rizzi, G., Cowan, A., Scott, C., Megill, J., Tirosh, B., 2016. CHO cells knocked out for TSC2 display an improved productivity of antibodies under fed batch conditions, 113 (9), 1942–1952. https://doi.org/10.1002/bit.25951.

Mellahi, K., Cambay, F., Brochu, D., Gilbert, M., Perrier, M., Ansorge, S., Henry, O., 2019. Process development for an inducible rituximab-expressing Chinese hamster ovary cell line. Biotechnol. Prog. 35 (1), e2742.

Moore, D., Sinilaite, A., Killikelly, A., 2022. Summary of the national advisory committee on immunization (NACI) statement update on the recommended use of palivizumab to reduce complications of respiratory syncytial virus infection in infants. Can. Commun. Dis. Rep. 48 (7-8), 363–366. https://doi.org/10.14745/ccdr.v48i78a08.

Mullick, A., Xu, Y., Warren, R., Koutroumanis, M., Guilbault, C., Broussau, S., Massie, B., 2006. The cumate gene-switch: a system for regulated expression in mammalian cells. BMC Biotechnol. 6 (1), 43. https://doi.org/10.1186/1472-6750-6-43.

Mulukutla, B.C., Gramer, M., Hu, W.-S., 2012. On metabolic shift to lactate consumption in fed-batch culture of mammalian cells. Metab. Eng. 14 (2), 138–149. https://doi.org/10.1016/j.ymben.2011.12.006.

Mulukutla, B.C., Khan, S., Lange, A., Hu, W.-S., 2010. Glucose metabolism in mammalian cell culture: new insights for tweaking vintage pathways. Trends Biotechnol. 28 (9), 476–484. https://doi.org/10.1016/j.tibtech.2010.06.005.

Muralidharan, N., Bolduc, Emma, Davis, M., 2024. Characterizing Oxygen Mass Transfer and Shear During Cell Culture: Calculating the Maximum Cell Density Supported By a 20,000-Liter Stirred-Tank Bioreactor. Bioprocess International. Retrieved 11-25-2024 from.

Nargund, S., Qiu, J., Goudar, C.T., 2015. Elucidating the role of copper in CHO cell energy metabolism using 13C metabolic flux analysis. Biotechnol. Prog. 31 (5), 1179–1186.

Nunez, R., Sancho-Martinez, S., Novoa, J., Lopez-Hernandez, F., 2010. Apoptotic volume decrease as a geometric determinant for cell dismantling into apoptotic bodies. Cell Death Differ. 17 (11), 1665–1671.

Orellana, C.A., Marcellin, E., Schulz, B.L., Nouwens, A.S., Gray, P.P., Nielsen, L.K., 2015. High-antibody-producing Chinese hamster ovary cells up-regulate intracellular protein transport and glutathione synthesis. J. Proteome Res. 14 (2), 609–618.

Ozturk, S.S., Palsson, B.Ø., 1990. Effects of dissolved oxygen on hybridoma cell growth, metabolism, and antibody production kinetics in continuous culture. Biotechnol. Prog. 6 (6), 437–446.

Ozturk, S.S., Riley, M.R., Palsson, B.O., 1992. Effects of ammonia and lactate on hybridoma growth, metabolism, and antibody production. Biotechnol. Bioeng. 39 (4), 418–431. https://doi.org/10.1002/bit.260390408.

Pan, X., Alsayyari, A.A., Dalm, C., Hageman, J.A., Wijffels, R.H., Martens, D.E., 2019. Transcriptome analysis of CHO cell size increase during a fed-batch process, 14 (3), 1800156. https://doi.org/10.1002/biot.201800156.

Pan, X., Dalm, C., Wijffels, R.H., Martens, D.E., 2017. Metabolic characterization of a CHO cell size increase phase in fed-batch cultures. Appl. Microbiol Biotechnol. 101 (22), 8101–8113. https://doi.org/10.1007/s00253-017-8531-y.

Pappenreiter, M., Sissolak, B., Sommeregger, W., Striedner, G., 2019. Oxygen uptake rate soft-sensing via dynamic k L a computation: cell volume and metabolic transition prediction in mammalian bioprocesses. Front. Bioeng. Biotechnol. 7, 195.

Pereira, S., Kildegaard, H.F., Andersen, M.R., 2018. Impact of CHO metabolism on cell growth and protein production: an overview of toxic and inhibiting metabolites and nutrients. Biotechnol. J. 13 (3), 1700499. https://doi.org/10.1002/biot.201700499.

Poulain, A., Mullick, A., Massie, B., Durocher, Y., 2019. Reducing recombinant protein expression during CHO pool selection enhances frequency of high-producing cells. J. Biotechnol. 296, 32–41. https://doi.org/10.1016/j.jbiotec.2019.03.009.

Poulain, A., Perret, S., Malenfant, F., Mullick, A., Massie, B., Durocher, Y., 2017. Rapid protein production from stable CHO cell pools using plasmid vector and the cumate gene-switch. J. Biotechnol. 255, 16–27. https://doi.org/10.1016/j.jbiotec.2017.06.009.

Rechmann, H., Friedrich, A., Forouzan, D., Barth, S., Schnabl, H., Biselli, M., Boehm, R., 2007. Characterization of photosynthetically active duckweed (Wolffia australiana) in vitro culture by respiration activity monitoring system (RAMOS). Biotechnol. Lett. 29, 971–977.

Reyes, S.J., Durocher, Y., Pham, P.L., Henry, O., 2022. Modern sensor tools and techniques for monitoring controlling improving cell culture processes. Processes 10 (2). https://doi.org/10.3390/pr10020189.

Reyes, S.J., Durocher, Y., Schulte, A., Keebler, M., Roy, M., Voyer, R., Pham, P.L.(2022). . Kuhner. Retrieved 2024-11-25 fromTransfer-rate Online Measurement (TOM) system for analyzing the respiratory activity of a Chinese Hamster Ovary (CHO) cell pool expressing SARS-CoV-2 Spike Protein⟨https://kuhner.com/wAssets/docs/download/Poster/Poster-NRC/TOM_CHO-POOL_POSTER_NRC_Kuhner.pdf⟩.

Reyes, S.J., Keebler, M., Schulte, A., Voyer, R., Durocher, Y., Henry, O., Pham, P.L., 2023. Impact of Protein Production on Metabolic Activity of Cho Stable Cell Line Producing Palivizumab. Kuhner. ⟨https://kuhner.com/wAssets/docs/download/Poster/Poster-NRC/TOM_Antibody_Poster-4_NRC-Kuhner.pdf⟩. Retrieved 2024-09-27 from.

Reyes, S.J., Lemire, L., Molina, R.S., Henry, O., Roy, M., L'Ecuyer-Coelho, H., Pham, P.L., 2024. Multivariate data analysis of process parameters affecting the growth and productivity of stable Chinese hamster ovary cell pools expressing SARS-CoV-2 spike protein as vaccine antigen in early process development. Biotechnol. Prog., e3467.

Reyes, S.J., Pham, P.L., Durocher, Y., Henry, O., 2024. CHO stable pool fed-batch process development of SARS-CoV-2 spike protein production: impact of aeration conditions and feeding strategies (n/a(n/a)). Biotechnol. Prog., e3507. https://doi.org/10.1002/btpr.3507.

Rico, J., Nantel, A., Pham, P.L., Voyer, R., Durocher, Y., Penny, S., Culf, E., 2018. Kinetic model of metabolism of monoclonal antibody producing CHO cells. Curr. Metab. 6 (3), 207–217.

Rish, A.J., Drennen, J.K., Anderson, C.A., 2022. Metabolic trends of Chinese hamster ovary cells in biopharmaceutical production under batch and fed-batch conditions. Biotechnol. Prog. 38 (1), e3220. https://doi.org/10.1002/btpr.3220.

Savizi, I.S.P., Maghsoudi, N., Motamedian, E., Lewis, N.E., Shojaosadati, S.A., 2022. Valine feeding reduces ammonia production through rearrangement of metabolic fluxes in central carbon metabolism of CHO cells. Appl. Microbiol Biotechnol. 106 (3), 1113–1126.

Scheidle, M., Klinger, J., Büchs, J., 2007. Combination of On-line pH and oxygen transfer rate measurement in shake flasks by fiber optical technique and respiration activity mo nitoring system (RAMOS). Sensors 7 (12), 3472–3480.

Seletzky, J.M., Noack, U., Hahn, S., Knoll, A., Amoabediny, G., Büchs, J., 2007. An experimental comparison of respiration measuring techniques in fermenters and shake flasks: exhaust gas analyzer vs. RAMOS device vs. respirometer. Journal of Industrial Microbiology Biotechnology 34 (2), 123–130.

Seletzky, J.M., Noak, U., Fricke, J., Welk, E., Eberhard, W., Knocke, C., Büchs, J., 2007. Scale-up from shake flasks to fermenters in batch and continuous mode with Corynebacterium glutamicum on lactic acid based on oxygen transfer and pH. Biotechnol. Bioeng. 98 (4), 800–811.

Sellick, C.A., Croxford, A.S., Maqsood, A.R., Stephens, G., Westerhoff, H.V., Goodacre, R., Dickson, A.J., 2011. Metabolite profiling of recombinant CHO cells: designing tailored feeding regimes that enhance recombinant antibody production. Biotechnol. Bioeng. 108 (12), 3025–3031. https://doi.org/10.1002/bit.23269.

Sellick, C.A., Croxford, A.S., Maqsood, A.R., Stephens, G.M., Westerhoff, H.V., Goodacre, R., Dickson, A.J., 2015. Metabolite profiling of CHO cells: molecular reflections of bioprocessing effectiveness. Biotechnol. J. 10 (9), 1434–1445. https://doi.org/10.1002/biot.201400664.

Shahabi, F., Abdoli, S., Bazi, Z., Shamsabadi, F., Yamchi, A., Shahbazi, M., 2023. Enhancing productivity of Chinese hamster ovary (CHO) cells: synergistic strategies combining low-temperature culture and mTORC1 signaling engineering. Front. Bioeng. Biotechnol. 11, 1268048.

Sheikholeslami, Z., Jolicoeur, M., Henry, O., 2013a. The impact of the timing of induction on the metabolism and productivity of CHO cells in culture. Biochem. Eng. J. 79, 162–171.

Sheikholeslami, Z., Jolicoeur, M., Henry, O., 2013b. Probing the metabolism of an inducible mammalian expression system using extracellular isotopomer analysis. J. Biotechnol. 164 (4), 469–478.

Stöckmann, C., Maier, U., Anderlei, T., Knocke, C., Gellissen, G., Büchs, J., 2003. The oxygen transfer rate as key parameter for the characterization of Hansenula polymorpha screening cultures. Journal of Industrial Microbiology Biotechnology 30 (10), 613–622.

Stuible, M., Gervais, C., Lord-Dufour, S., Perret, S., L'Abbé, D., Schrag, J., Durocher, Y., 2021. Rapid, high-yield production of full-length SARS-CoV-2 spike ectodomain by transient gene expression in CHO cells. J. Biotechnol. 326, 21–27. https://doi.org/10.1016/j.jbiotec.2020.12.005.

Tait, A.S., Tarrant, R.D., Velez-Suberbie, M.L., Spencer, D.I., Bracewell, D.G., 2013. Differential response in downstream processing of CHO cells grown under mild hypothermic conditions. Biotechnol. Prog. 29 (3), 688–696.

Templeton, N., Dean, J., Reddy, P., Young, J.D., 2013. Peak antibody production is associated with increased oxidative metabolism in an industrially relevant fed-batch CHO cell culture. Biotechnol. Bioeng. 110 (7), 2013–2024. https://doi.org/10.1002/bit.24858.

Traustason, B., 2019. Amino acid requirements of the Chinese hamster ovary cell metabolism during recombinant protein production. BioRxiv, 796402.

Trummer, E., Fauland, K., Seidinger, S., Schriebl, K., Lattenmayer, C., Kunert, R., Katinger, H., 2006. Process parameter shifting: Part I. Effect of DOT, pH, and temperature on the performance of Epo-Fc expressing CHO cells cultivated in controlled batch bioreactors. Biotechnol. Bioeng. 94 (6), 1033–1044.

Wagner, B.A., Venkataraman, S., Buettner, G.R., 2011. The rate of oxygen utilization by cells. Free Radic. Biol. Med. 51 (3), 700–712.

Wallocha, T., Popp, O., 2021. Off-gas-based soft sensor for real-time monitoring of biomass and metabolism in Chinese hamster ovary cell continuous processes in single-use bioreactors. Processes 9 (11), 2073.

Wang, X., Zhou, G., Liang, L., Liu, Y., Luo, A., Wen, Z., Wang, X.Z., 2024. Deep learning-based image analysis for in situ microscopic imaging of cell culture process. Eng. Appl. Artif. Intell. 129, 107621.

Wilkens, C.A., Altamirano, C., Gerdtzen, Z.P., 2011. Comparative metabolic analysis of lactate for CHO cells in glucose and galactose. Biotechnol. Bioprocess Eng. 16, 714–724.

Xing, Z., Kenty, B., Koyrakh, I., Borys, M., Pan, S.-H., Li, Z.J., 2011. Optimizing amino acid composition of CHO cell culture media for a fusion protein production. Process Biochem. 46 (7), 1423–1429.

Xu, W.-J., Lin, Y., Mi, C.-L., Pang, J.-Y., Wang, T.-Y., 2023. Progress in fed-batch culture for recombinant protein production in CHO cells. Appl. Microbiol. Biotechnol. 107 (4), 1063–1075.

Xu, J., Tang, P., Yongky, A., Drew, B., Borys, M.C., Liu, S., Li, Z.J., 2019. Systematic development of temperature shift strategies for Chinese hamster ovary cells based on short duration cultures and kinetic modeling. MAbs 11 (1), 191–204. https://doi.org/10.1080/19420862.2018.1525262.

Yallop, C.A., Svendsen, I., 2001. The effects of G418 on the growth and metabolism of recombinant mammalian cell lines. Cytotechnology 35, 101–114.

Zagari, F., Jordan, M., Stettler, M., Broly, H., Wurm, F.M., 2013. Lactate metabolism shift in CHO cell culture: the role of mitochondrial oxidative activity. N. Biotechnol. 30 (2), 238–245. https://doi.org/10.1016/j.nbt.2012.05.021.

Zalai, D., Hevér, H., Lovász, K., Molnár, D., Wechselberger, P., Hofer, A., Herwig, C., 2016. A control strategy to investigate the relationship between specific productivity and high-mannose glycoforms in CHO cells. Appl. Microbiol Biotechnol. 100 (16), 7011–7024. https://doi.org/10.1007/s00253-016-7380-4.

Zhang, L.-x, Zhang, W.-y, Wang, C., Liu, J.-t, Deng, X.-c, Liu, X.-p, Tan, W.-s, 2016. Responses of CHO-DHFR cells to ratio of asparagine to glutamine in feed media: cell growth, antibody production, metabolic waste, glutamate, and energy metabolism. Bioresour. Bioprocess. 3, 1–12.

Zhou, W., Hu, W.S., 1994. On-line characterization of a hybridoma cell culture process. Biotechnol. Bioeng. 44 (2), 170–177.

Zhou, W., Rehm, J., Hu, W.S., 1995. High viable cell concentration fed-batch cultures of hybridoma cells through on-line nutrient feeding. Biotechnol. Bioeng. 46 (6), 579–587.

Zhu, Z., Chen, X., Li, W., Zhuang, Y., Zhao, Y., Wang, G., 2023. Understanding the effect of temperature downshift on CHO cell growth, antibody titer and product quality by intracellular metabolite profiling and in vivo monitoring of redox state. Biotechnol. Prog. 39 (4), e3352. https://doi.org/10.1002/btpr.3352.

Zimmermann, H.F., Anderlei, T., Büchs, J., Binder, M., 2006. Oxygen limitation is a pitfall during screening for industrial strains. Appl. Microbiol. Biotechnol. 72, 1157–1160.